Published in final edited form as:
Cell Mol Bioeng. 2011 June 1; 4(2): 281–301. doi:10.1007/s12195-011-0162-2.

Regulation of Adipose Tissue Metabolism in Humans: Analysis of Responses to the Hyperinsulinemic-Euglycemic Clamp Experiment

Jaeyeon Kim[1,2,3], **Gerald M. Saidel**[1,2], and **Satish C. Kalhan**[2,3]

[1]Department of Biomedical Engineering, Case Western Reserve University, Cleveland, OH 44106, USA

[2]Center for Modeling Integrated Metabolic Systems, Case Western Reserve University, Cleveland, OH 44106, USA

[3]Department of Pathobiology, Lerner Research Institute, NE4-203, Cleveland Clinic Foundation, 9500 Euclid Avenue, Cleveland, OH 44195, USA

Abstract

The suppression of lipolysis is one of the key metabolic responses of the adipose tissue during hyperinsulinemia. The failure to respond and resulting increase in plasma fatty acids could contribute to the development of insulin resistance and perturbations in the fuel homeostasis in the whole body. In this study, a mechanistic, computational model of adipose tissue metabolism *in vivo* has been enhanced to simulate the physiological responses during hyperinsulinemic-euglycemic clamp experiment in humans. The model incorporates metabolic intermediates and pathways that are important in the fed state. In addition, it takes into account the heterogeneity of triose phosphate pools (glycolytic vs. glyceroneogenic), within the adipose tissue. The model can simulate not only steady-state responses at different insulin levels, but also concentration dynamics of major metabolites in the adipose tissue venous blood in accord with the *in vivo* data. Simulations indicate that (1) regulation of lipoprotein lipase (LPL) reaction is important when the intracellular lipolysis is suppressed by insulin; (2) intracellular diglyceride levels can affect the regulatory mechanisms; and (3) glyceroneogenesis is the dominant pathway for glycerol-3-phosphate synthesis even in the presence of increased glucose uptake by the adipose tissue. Reduced redox and increased phosphorylation states provide a favorable milieu for glyceroneogenesis in response to insulin. A parameter sensitivity analysis predicts that insulin-stimulated glucose uptake would be more severely affected by impairment of GLUT4 translocation and glycolysis than by impairment of glycogen synthesis and pyruvate oxidation. Finally, simulations predict metabolic responses to altered expression of phosphoenolpyruvate carboxykinase (PEP-CK). Specifically, the increase in the rate of re-esterification of fatty acids observed experimentally with the overexpression of PEPCK in the adipose tissue would be accompanied by the up-regulation of acyl Co-A synthase.

Keywords

Lipolysis; Re-esterification; Insulin; TG-FA cycle; Mathematical model

Address correspondence to Satish C. Kalhan, Department of Pathobiology, Lerner Research Institute, NE4-203, Cleveland Clinic Foundation, 9500 Euclid Avenue, Cleveland, OH 44195, USA. sck@case.edu.

INTRODUCTION

As one of the most potent antilipolytic hormones, insulin suppresses the breakdown of triglycerides (TG) in the adipose tissue. Since the breakdown of TG is regulated by a complex mechanism involving various lipases and other proteins,[23,42] its suppression by insulin would require the modulation of these regulatory steps. Studies in transgenic animals suggest that hormone sensitive lipase (HSL), adipose triglyceride lipase (ATGL) and perilipin A are the major regulators of intracellular lipolysis.[16,17,51] Insulin can suppress lipolysis by modulating the activities of these proteins. It transcriptionally down-regulates the activity of ATGL,[20] and acutely affects the activities of HSL and perilipin A by promoting their dephosphorylation via two different mechanisms.[5,46] It reduces the levels of cyclic AMP (cAMP) by activating phosphodiesterase (PDB). In addition, protein phosphatase 1 (PP1) is activated by insulin dephosphorylating HSL and perilipin directly. Even though the activity of ATGL can only be regulated transcriptionally, the TG breakdown by ATGL can be affected indirectly via dephosphorylation of perilipin. While insulin can suppress the breakdown of TG and diglycerides (DG) via different cellular mechanisms, it is not certain whether the lipolytic reactions catalyzed by different lipases are equally suppressed by the action of insulin. Using a computational model of adipose tissue metabolism developed previously,[21] we have shown differential activation of various lipolytic reactions by epinephrine. The integrated response of these systems, i.e. lipolytic pathways in response to insulin, needs to be examined.

The synthesis of TG in adipose tissue requires a source of glycerol-3-phospahte (G3P). Either glucose or pyruvate (and alanine, lactate) can be utilized for the synthesis of G3P. Since adipose tissue has very low activity of glycerol kinase, it cannot utilize glycerol in significant quantities to synthesize G3P. G3P is synthesized from pyruvate (or lactate) via glyceroneogenesis. [36] Studies in rats suggest that glyceroneogenesis is the dominant pathway for the synthesis of G3P in the adipose tissue even when the rate of glucose uptake is significant.[31] The utilization of pyruvate or lactate for the synthesis of G3P via different pools of triose phosphates in the adipose tissue could help reconcile these apparently discrepant data. In our previous model of adipose tissue metabolism, we have described the intracellular utilization of pyruvate by incorporating two separate pathways for the synthesis of G3P. We did not consider the possibility of two separate pools of triose phosphates. The incorporation of two separate domains (i.e., heterogeneity) of triose phosphates would enhance our understanding of the regulation of glyceroneogenesis and TG synthesis.

Cytosolic Phosphoenolpyruvate carboxykinase (PEPCK) is a key regulatory enzyme for glyceroneogenesis. Increased activity of PEPCK in adipose tissue is associated with obesity.[7] Indeed, PEPCK is one of the primary targets for anti-diabetic drugs, thiazolidinediones (TZDs) due to its critical role in the regulation of re-esterification of fatty acid (FA).[52] As shown in transgenic mice studies, the overexpression of PEPCK in the adipose tissue results in obesity in these mice without insulin resistance.[13] The increased rate of re-esterification of FA results in a decreased rate of FA release into circulation and lowering of the plasma levels of FA in these animals. In addition to changes in PEPCK activity, the availability of substrates can also regulate the flux through glyceroneogenesis. Despite the importance of glyceroneogenesis in the regulation of TG synthesis, definitive *in vivo* studies have not been performed. Thus, the regulatory mechanism for increased glyceroneogenesis in response to insulin remains uncertain.

In the present study, we have modified our previously described computational model of adipose tissue metabolism[21] to simulate responses to insulin plus glucose. Specifically, we have (1) examined the suppression of various lipolytic reactions by insulin; (2) investigated the mechanisms that regulate the flux through glyceroneogenesis in response to insulin/

glucose infusion; (3) examined the effect of increasing the arterial levels of lactate (substrates); and (4) examined the effect of change in PEPCK activity on glyceroneogenesis and re-esterification of FA. Our hypothesis is that breakdown of TG and DG by ATGL and HSL are differentially suppressed by the action of insulin. We postulate that distinctive changes in the levels of lipolytic intermediates (i.e., DG and monoglycerides, MG) result from the differential suppression of lipolytic reactions by insulin. Furthermore, we expect that glyceroneogenesis increases in response to insulin due to the increased availability of pyruvate as well as favorable states of cellular redox (i.e., $NADH/NAD^+$) and phosphorylation (i.e., ATP/ADP). With respect to the effect of increased substrate availability, we expect that increased levels of lactate facilitate the accretion of fat into the adipose tissue. Finally, the model is used to predict physiological responses from overexpressed PEPCK in the adipose tissue to address whether higher PEPCK activity is sufficient to increase the rate of re-esterification of FA or whether induction of additional enzymes is required. With this model, we examine the effect of increasing the activity of acyl CoA synthetase (ACS) on the rate of FA re-esterification and its importance on the synthesis of fatty acyl CoA (FAC), a co-substrate for TG synthesis.

METHODS

Hyperinsulinemic-euglycemic clamp experiment in humans is an effective method for investigating the regulation of TG breakdown by insulin. This technique has been widely used for quantifying insulin resistance *in vivo*. Following a constant rate infusion of insulin, resulting in constant plasma insulin levels, the plasma glucose concentration is maintained in the euglycemic range by infusing glucose at varying rates. The rate of infusion of glucose at steady state is a measure of insulin sensitivity. To simulate the responses associated with such a perturbation, an earlier model of adipose tissue metabolism *in vivo*[21] in the fasting state was enhanced by incorporating additional metabolic intermediates and metabolic steps that are considered significant in the fed state.

Metabolites, Pathways, and Cellular Distribution (Assumptions)

Insulin stimulates glucose uptake in adipose tissue by increasing the translocation of glucose transporter 4 (GLUT4) to the plasma membrane.[2] Insulin also increases reaction fluxes through several intracellular metabolic pathways e.g. glycogen synthesis,[25] glycolysis [1,24,25] and lipogenesis[29] *etc*. By suppressing cAMP formation or activating PP1, insulin can activate multiple enzymes in the glycolytic pathways including glycogen synthase,[25] hexokinase,[25] phosphofructokinase, [1] pyruvate kinase,[1] and pyruvate dehydrogenase. [24] Stimulation of fatty acid synthesis from glucose (*de novo* lipogenesis) requires a source of NADPH. The primary source of NADPH is the pentose phosphate pathway where NADPH is generated when glucose-6-phosphate is oxidized to ribulose-5-phospahte (R5P). R5P re-enters the glycolytic pathway at the level of fructose-6-phosphate (F6P) and GAP. By incorporating F6P, glycogen (GLY), R5P, $NADP^+$ and NADPH, the model can be used to describe the glycogen cycle, pentose phosphate pathway and *de novo* lipogenesis (Fig. 1).

Following the strategy for modeling the metabolic reaction network that we used previously to reduce model complexity,[21] several metabolic reaction steps were combined to form at least one irreversible reaction; otherwise, reactions are reversible (Fig. 1). We assume that insulin activates or inhibits a certain reaction step only if it has been shown that insulin can modulate one of the enzyme activities involved in the lumped reactions. Since no mechanisms are known by which insulin can regulate the activities of enzymes for fully reversible reactions (e.g., glucose-6-phosphate isomerase, lactate dehydrogenase and glycerol-3-phosphate dehydrogenase), the model does not consider these reactions to be stimulated by insulin. In our model (Fig. 1), insulin can activate the following reactions: glucose to glucose-6-phosphate by hexokinase, fructose-6-phosphate (F6P) to

glyceraldehyde-3-phosphate (GAP) by phosphofructokinase, GAP to pyruvate by pyruvate kinase, pyruvate oxidation by pyruvate dehydrogenase and glycogen synthesis by glycogen synthase. Also, insulin can inhibit the following reactions: lipolysis,[5,46] glycogen phosphorylation [50] and proteolysis.[39]

Data from studies in humans show that there is a net uptake of glucose by the adipose tissue both in the fasting and in the fed states.[10,18] These data have been used to suggest that glycerol-3-phosphate (G3P) is synthesized from glucose in the adipose tissue. However, recent data in rat show that pyruvate (via glyceroneogenesis) is the dominant carbon source of G3P.[31] Such data would indicate the existence of two distinct pools of G3P within adipose tissue, a glycolytic pool and a glyceroneogenic pool. In the following enhanced model, the heterogeneity associated with the triose phosphates are considered to be localized in distinct cellular subdomains: either glycolytic (GAP1 and G3P1) or glyceroneogenic (GAP2 and G3P2).

Blood flow to the adipose tissue increases with insulin.[19] Therefore, blood flow in adipose tissue is given as a model input together with the arterial levels of metabolites.

Dynamics Mass Balances of Substrates

Substrate transport and metabolic reaction dynamics in blood and in cellular compartments are represented by mass balance equations. In the blood compartment of volume V_b, the concentration $C_{b,i}$ of the substrate i changes with time:

$$V_b \frac{dC_{b,i}}{dt} = Q(t)\left[C_{a,i}(t) - C_{b,i}\right] + R_{b,i} - J_{b\leftrightarrow c,i} \quad (1)$$

where $J_{b\leftrightarrow c,i}$ is the net mass transport rates from blood to cells, and $R_{b,i}$ is the net reaction rate. The arterial concentration, $C_{a,i}(t)$ and the blood flow, $Q(t)$ are given as input functions as specified from experiments. The concentration, $C_{c,i}$ substrate i in the cellular compartment changes with time:

$$V_{c,i} \frac{dC_{c,i}}{dt} = R_{c,i} + J_{b\leftrightarrow c,i} \quad (2)$$

where $R_{c,i}$ is the net reaction rate in the cellular compartment and $V_{c,i}$ is the volume of the cellular compartment occupied by substrate i.

Transport and Metabolic Fluxes

For passive simple diffusion of glycerol, FA, O_2 and CO_2 between blood and cellular domains, the general transport flux is:

$$J_{b\leftrightarrow c,i} = \gamma_i\left[C_{b,i} - C_{c,i}\right] \quad (3)$$

where γ_i is the mass transport coefficient of substrate i. For carrier-mediated facilitated transport of glucose, pyruvate, lactate, and alanine, the general transport flux is:

$$J_{b\leftrightarrow c,i} = T_{max,i}\left(\frac{C_{b,i}}{M_{m,i} + C_{b,i}} - \frac{C_{c,i}}{M_{m,i} + C_{c,i}}\right) \quad (4)$$

where $T_{max,i}$ is the maximum mass transport coefficient of substrate i and $M_{m,i}$ is the Michaelis–Menten (M–M) constant of substrate i.

The net reaction rates ($R_{x,i}$) involve one or more metabolic reaction fluxes (φ_k), which are complex nonlinear functions of substrate concentrations (Appendix 1). For those reactions far from thermodynamic equilibrium, the reaction flux, φ_k is represented by a general irreversible bi-bi substrate-to-product enzymatic reaction coupled with controller energy metabolite pairs:

$$\varphi_k = V_{max,k}\left(\frac{PS^{\pm}}{\mu^{\pm}+PS^{\pm}}\right)\left(\frac{RS_1^{\pm}}{\nu^{\pm}+RS_1^{\pm}}\right)\left(\frac{RS_2^{\pm}}{\eta^{\pm}+RS_2^{\pm}}\right)\times\left(\frac{C_X \cdot C_Y}{K_{m,k}+C_V \cdot C_W \cdot K_{m,k}/K_{i,k}+C_X \cdot C_Y}\right) \quad (5)$$

where C_X, C_Y, C_V, and C_W are reactant and product concentrations; $V_{max,k}$ is the maximum rate coefficient and $K_{m,k}$ is a phenomenological M–M constant; PS^+ ($=C_{ATP}/C_{ADP}$), $RS_1^+(=C_{NADH}/C_{NAD^+})$ and $RS_2^+(=C_{NADPH}/C_{NADP^+})$ indicate the cellular phosphorylation and redox states. For some reactions, the effect of these controllers can be in the opposite direction (viz., $PS^- = 1/PS^+$, $RS_1^- = 1/RS_1^+$ and $RS_2^- = 1/RS_2^+$). In addition, $\mu^{\pm}$, $\nu^{\pm}$ and $\eta^{\pm}$ are parameters for the metabolic controllers.

The reactions that are close to thermodynamic equilibrium and reversible are represented by the flux relationship:

$$\varphi_k = \left(\frac{V_{f,k}\frac{C_X \cdot C_Y}{K_{f,k}} - V_{b,k}\frac{C_V \cdot C_W}{K_{b,k}}}{1+\frac{C_X \cdot C_Y}{K_{f,k}}+\frac{C_V \cdot C_W}{K_{b,k}}}\right) \quad (6)$$

where $V_{f,k}$ and $V_{b,k}$ are the forward and reverse rate coefficients; $K_{f,k}$ and $K_{b,k}$ are the phenomenological M–M constants for reactants and products. The forward and reverse rate coefficients are related by Haldane relationship. The reversible reactions are those catalyzed by lactate dehydrogenase, G3P dehydrogenase, and glucose-6-phosphate (G6P) isomerase.

Insulin Modulation of Fluxes

The translocation of glucose transporter and several metabolic fluxes are modulated by the action of insulin. The increase in the rate of glucose uptake by the adipose tissue, however, is significantly delayed in response to insulin. The delay in the action of insulin is related to the transport of insulin from the plasma to the interstitium across vascular endothelium,[55] and the translocation of GLUT4 to the plasma membrane. [30] Activation of the intermediary proteins in the insulin signaling cascade is considered to be instantaneous. [15] Thus, the interstitial level of insulin, $C_I(t)$ that modulates the cellular processes changes with time according to

$$C_I(t) = C_I(0) + [C_I(\infty) - C_I(0)][1 - \exp(-t/\tau)] \quad (7)$$

where τ is the time constant and $C_I(\infty)$ is the steady-state value. The interstitial concentration of insulin was set equal to 21% of its plasma level.[4]

The maximum glucose transport coefficient, $T_{max,GLC}$ dynamically changes depending on interstitial insulin concentration:

$$\frac{dT_{max,GLC}}{dt} = 1 + \theta C_I(t) - [1 + \theta C_I(0)]\frac{T_{max,GLC}(t)}{T_{max,GLC}(0)} \quad (8)$$

where θ is the parameter indicating the degree of activation by insulin and initially, $T_{max,GLC}(0)$. When C_I reaches a steady state, then $T_{max,GLC}(t)$ will reach a constant value.

Changes in the rate coefficients of other metabolic fluxes are assumed to be relatively fast and related to $C_I(t)$. For the metabolic reactions that are activated by insulin, glycolysis ($\varphi_{GLC\rightarrow G6P}$, $\varphi_{F6P\rightarrow GAP}$, $\varphi_{GAP\rightarrow PYR}$), glycogen synthesis ($\varphi_{G6P\rightarrow GLY}$) and pyruvate oxidation ($\varphi_{PYR\rightarrow ACoA}$), the reaction rate coefficients increase with insulin concentration:

$$V^{+}_{max,k}=V^{0}_{max,k}\left(1+\lambda_k\frac{[C_I(t)-C_I(0)]^2}{C_I(0)^2+[C_I(t)-C_I(0)]^2}\right) \quad (9)$$

where $V^{0}_{max,k}$ is the basal state maximum rate coefficient and λ_k indicates the degree of activation for a corresponding reaction by insulin. For reactions that are suppressed, viz., glycogenolysis ($\varphi_{GLY\rightarrow G6P}$), proteolysis ($\varphi_{PRT\rightarrow ALA}$) and lipolysis ($\varphi_{TG\rightarrow DG,ATGL}$, $\varphi_{TG\rightarrow DG,HSL}$, $\varphi_{DG\rightarrow MG,HSL}$), the reaction rate coefficients decrease with insulin concentration:

$$V^{-}_{max,k}=V^{0}_{max,k}\left(\frac{\alpha_k}{\alpha_k+C_I(t)^2}\right) \quad (10)$$

where α_k indicates the degree of suppression.

Parameter Estimation and Simulation Strategy

Values of substrate concentrations, transport and metabolic fluxes, and associated model parameters in the basal state (Tables 1, 2, and 3) were based on previous analysis.[21] In this study, we used the same fluxes and parameters related to the mass transport between blood and cellular compartments. As a consequence of adding pathways and metabolic intermediates to the model, values of some of intracellular metabolic fluxes and model parameters were modified.

The parameters related to suppression of the lipolytic reactions (i.e., α_k) were determined first by simulating steady-state insulin dose–response data from *in vivo* human studies.[48] These reactions are independent of the parameters that modulate glucose metabolism. Simulated steady-state responses to different levels of plasma insulin [35 pM, 113 pM and 383 pM] were examined. Additional inputs to the model for steady state simulations include arterial glycerol and FA concentrations. Simulated concentrations of glycerol in the venous effluent blood were compared with experimental data. From empirical simulation studies, we found consistent results when parameters related to suppression of the lipolytic reactions (i.e., α_k) were set to the square of interstitial insulin concentration in the basal state (i.e., $C_I(0)^2$ = 70.6 pM^2) for TG and DG breakdowns by ATGL and HSL ($\varphi_{TG\rightarrow DG,ATGL}$, $\varphi_{TG\rightarrow DG,HSL}$, $\varphi_{DG\rightarrow MG,HSL}$).

After successful evaluation of the model parameters (i.e., α_k), simulated responses were compared with data from hyperinsulinemic-euglycemic clamp in humans. Corresponding to *in vivo* studies,[8,9] we simulated responses to a constant rate infusion of insulin [35 mU/ m^2/ min] administered intravenously for 120 min. Based on *in vivo* data,[55] a time constant of 10 min was assumed so that the interstitial levels of insulin reached a steady state around 30 min in response to a step increase in the plasma insulin levels from 40 pM to 350 pM (Fig. 2). Adipose blood flow $Q(t)$ and arterial concentration dynamics $C_{a,k}(t)$ of glucose, lactate, glycerol, FA, and TG were input functions (Fig. 3).

The variable rate of infusion of exogenous glucose required to maintain constant levels of glucose is modeled by the input functions for arterial glucose concentrations as listed in Table 4. Optimal estimates of the model parameters (Table 5) related to insulin action (i.e., λ_k) were obtained by comparison of simulated outputs with data from *in vivo* human

studies.[8,9] Parameters related to suppression of the lipolytic reactions (i.e., a_k) were set to the square of interstitial insulin concentration in the basal state (i.e., $C_I(0)^2 = 70.6$ pM^2) for TG and DG breakdowns by ATGL and HSL ($\varphi_{TG\rightarrow DG,ATGL}$, $\varphi_{TG\rightarrow DG,HSL}$, $\varphi_{DG\rightarrow MG,HSL}$).

Model simulations were performed under many physiological and/or metabolic conditions. The model equations were solved numerically using an integrator for stiff, ordinary differential equations, 'ode15 s' (MATLAB®, MathWorks Inc.). Optimal least-squares estimates of the model and input parameters were obtained using 'lsqcurvefit' (MATLAB®).

RESULTS

Steady-State Analysis of the Insulin Dose Response

The levels of glycerol in the venous blood draining the adipose tissue have been used as estimates of total TG breakdown. Glycerol released from TG breakdown cannot be used in adipose tissue due to the low activity of glycerol kinase. The steady-state responses to increasing dose of insulin were simulated by (1) examining the changes in the levels of glycerol in the venous blood as indicative of total TG breakdown: (2) estimating the rate of release of FA from TG breakdown; and (3) evaluating the rate of re-esterification of FA. The venous blood levels of glycerol decreased exponentially from 203 μM to 55 μM with increasing levels of insulin from 35 pM to 383 pM (Fig. 4a). Model simulations correspond to experimental data up to the level of plasma insulin of 113 pM. At the highest insulin level [383 pM], the simulated venous glycerol concentration was about 35% higher than the experimental data. However, when the plasma TG breakdown was completely suppressed by setting the maximum rate coefficient for LPL reaction to zero, model simulations were in good agreement with the published experimental data (Fig. 4a).

The rate of intracellular lipolysis (i.e., FA release from the breakdown of intracellular TG, DG and MG) decreased from 11.6 to 0.9 μmol/kg/min (Fig. 4b) in response to increasing insulin concentrations. The rate of total lipolysis (i.e., intracellular lipolysis plus plasma TG hydrolysis by LPL) showed a similar response. The fractional contribution of LPL mediated lipolysis to total lipolysis was higher at high insulin concentration (~5% at 35 pM insulin to ~40% at 383 pM insulin). There was no significant change in the intracellular re-esterification of FA with increasing concentrations of insulin. As a consequence, the fractional rate of intracellular re-esterification of FA released from TG breakdown increased from ~11% to ~112%. Total fractional re-esterification of FA changed from ~10% to ~75%.

Simulation of Hyperinsulinemic-euglycemic Clamp

Model Input Functions—Experimental data were used to generate the various continuous input functions for the model (Table 4).[55] With a constant rate of infusion of insulin (35 mU/m^2/ min), the plasma level of insulin showed a step increase (Fig. 2) reaching a steady state value of 350 pM by 15 min corresponding to data.[8] The simulated interstitial levels of insulin increased from 8.4 pM to 73.5 pM (Fig. 2). During the hyperinsulinemic clamp experiment, the arterial glucose concentration varied by ~10% (Fig. 3a), which was account for in the model simulation. The arterial lactate showed a sigmoidal increase (~40%) reaching a steady state at 30 min (Fig. 3b). The levels of arterial glycerol and FA decreased exponentially by ~60% and ~90%, respectively (Figs. 3c and 3d). Also, the arterial levels of TG decreased linearly by ~20% (Fig. 3e). The infusion of glucose and insulin resulted in a temporal increase in adipose blood flow reaching a maximum (2.5-fold increase) at ~30 min and slowly returning to the basal value over the next 90 min (Fig. 3f).

Venous Concentration Dynamics—By varying the levels of arterial substrates and adipose tissue blood flow, we simulated the concentration dynamics of metabolic substrates

in the venous blood draining the adipose tissue bed. The parameter values related to insulin action (i.e., λ_k) were optimally estimated (Table 5) by comparison of simulations with experimental data. Following the initiation of insulin infusion, the venous glucose levels decreased by 10 ~ 20% reaching a steady state at 30 min, whereas the venous lactate levels showed a sharp sigmoidal increase (~40%) for 30 min followed by a slow increase (Figs. 5a and 5b). The suppression of lipolysis by insulin resulted in exponential decreases in both FA and glycerol in the venous effluent that reached steady-state levels after 30 min. While glycerol concentration decreased to ~28% of the basal state, FA concentration in the venous blood decreased to ~12% (Figs. 5c and 5d). Also, venous TG levels decreased linearly by ~20% at 120 min (Fig. 5e). The simulated venous concentration dynamics of various substrates were in good agreement with data from *in vivo* studies.

Regulation of Lipolysis

Insulin suppresses the lipolytic reactions catalyzed by ATGL and HSL by different cellular mechanisms (viz., TG breakdown by ATGL (perilipin) vs. TG and DG breakdown by HSL). Since a_k value in the model (Eq. (10)) represents the degree of suppression by insulin, the differential suppression of lipolytic reactions was simulated using a larger a_k value [635 pM^2] for the ATGL reaction than the a_k values [70.6 pM^2] for the HSL reactions. For uniform suppression of lipolysis by insulin, the same a_k values [70.6 pM^2] were applied for all lipolytic reactions. ATGL and HSL reactions decreased ~97% from the basal rates with uniform suppression (Fig. 6a), whereas ATGL reaction with differential suppression was reduced by ~87%. These simulations were compared with those in which TG breakdown by ATGL was not suppressed. Changes in a_k for the ATGL reaction affected the venous FA concentration only when ATGL was not suppressed by insulin (Fig. 6b). However, the intracellular DG levels showed distinctive responses depending on the relative suppression of ATGL and HSL reactions (Fig. 6c). With uniform suppression of ATGL and HSL, the concentrations of DG decreased linearly by ~50 μM in 120 min. With differential suppression of the ATGL reaction, DG changed only after 60 min. Without suppression of the ATGL reaction, DG increased linearly ~20% after 120 min. With or without suppression of the ATGL reaction, MG exponentially decreased from 200 μM to 30 μM (simulation not shown).

Sources of G3P and Regulation of Glyceroneogenesis

Model simulations were used to predict the contributions of glycolysis and glyceroneogenesis to the synthesis of G3P required for the re-esterification of FA during the hyperinsulinemic-euglycemic clamp experiment. *In vivo* data have shown the dominant role of glyceroneogenesis for triglyceride synthesis in the basal state (10–13). To simulate the effect of effect of varying contribution of glycolysis and glyceroneogenesis to G3P synthesis during hyperinsulinemic euglycemic state, we used three different ratios of glycolytic and glyceroneogenic fluxes (Fig. 7). The rates of G3P synthesis via glycolysis and via glyceroneogenesis were normalized to their rates in the basal state. As shown in Fig. 7a, glyceroneogenesis increased by ~70% regardless of the absolute flux rate in the basal state, whereas the direct glycolytic contribution showed less increase (~35%) and even decreased by ~20% with increasing glycolytic contribution. Thus, the total rate of G3P synthesis (both glycolytic and glyceroneogenic) decreased by ~40% (from ~0.75 mmol/kg/min to ~0.49 mmol/kg/min) by 2 h of insulin infusion (Fig. 7b). Driving forces for the increased glyceroneogenesis were the increased cellular phosphorylation state indicated by ~40% higher C_{ATP}/C_{ADP} and the decreased (i.e., reduced) cellular redox state indicated by ~40% lower C_{NAD^+}/C_{NADH} (Fig. 7c).

Since lactate is one of the important precursors for glyceroneogenesis and is elevated with obesity, the effect of arterial lactate levels on glyceroneogenesis was examined *in silico*.

When arterial lactate concentrations were increased from 0.7 mM to 1.5 mM, the rate of glyceroneogenesis increased ~15% from 0.38 μmol/ kg/min and the rate of re-esterification increased ~10% from 1.27 μmol/kg/min (simulation not shown).

Effect of Reduced Insulin Action

Model simulations (Fig. 8) show the effects of reduced insulin action on glucose transport ($\lambda_{T_{max,GLC}}$ in $J_{b\leftrightarrow c,GLC}$), glycolysis ($\lambda_{Glycolysis}$ in $\varphi_{GLC\rightarrow G6P}$, $\varphi_{F6P\rightarrow GAP}$ and $\varphi_{GAP\rightarrow PYR}$), glycogen synthesis ($\lambda_{Glycogen\ Synthesis}$ in $\varphi_{G6P\rightarrow GLY}$) and pyruvate oxidation (λ_{PDH} in $\varphi_{PYR\rightarrow ACoA}$). These λ_k parameters, which are related to the stimulatory insulin action, were decreased to 20% of the reference values. The rate of glucose uptake by the adipose tissue decreased (from 9.8 μmol/kg/min) by ~30% from lower $\lambda_{T_{max,GLC}}$, by ~60% from lower $\lambda_{Glycolysis}$, by ~15% from lower $\lambda_{Glycogen\ Synthesis}$, and by ~1% from lower λ_{PDH}.

Simulations also showed the effect of reduced insulin action on the lactate release rate (negative) from adipose tissue (Fig. 9). Decreasing the λ_k parameters by 40% had distinctly different effects. The lactate release rate was reduced by 21% with decreased $\lambda_{T_{max,GLC}}$ and by 62% with decreased $\lambda_{Glycolysis}$. In contrast, it was increased by 31% with decreased $\lambda_{Glycogen\ Synthesis}$ and increased by 7% with decreased λ_{PDH} increased.

Effect of Altered PEPCK and ACS Expressions

The importance of PEPCK activity in the re-esterification of FA was examined by *in silico* transgenic experiments with model simulations that predicted the responses to altered enzyme expressions. The activity of PEPCK (i.e., $V_{max,PYR\rightarrow GAP2}$) was modulated in the basal state to determine its effects on the rates of glyceroneogenesis and FA release from adipose tissue into the circulation (Fig. 10). A 3-fold increase in PEPCK activity (i.e., $3\cdot V_{max,PYR\rightarrow GAP2}$) increased flux through glyceroneogenesis by ~70% (from 0.38 to 0.65 μmol/kg/min), but did not affect the rate of release of FA. However, when the activities of both acyl CoA synthetase (ACS) and PEPCK were increased two fold (i.e., $2\cdot V_{max,FA\rightarrow FAC}$), there was ~12% decrease in the FA release (8.6 μmol/kg/min) and the rate of glyceroneogenesis increased more than two folds.

DISCUSSION

Comparison of model simulations with experimental data provides confidence in the validity of this mechanistic model of adipose tissue metabolism. Consequently, the model is expected to simulate a variety of responses under conditions for which no experimental data is currently available. This study focuses on the regulation of lipolysis and re-esterification by insulin. Simulations indicate the significance of regulating LPL reactions with the suppressed intracellular lipolysis. Differential suppression of lipolytic reactions is not evident based on the dynamic changes in the venous concentrations of FA and glycerol, but the changes in DG level may suggest the differential regulation by insulin. In accord with experimental data, simulations show glyceroneogenesis to be the dominant pathway for G3P synthesis even when the glucose uptake by the adipose tissue increases. Elevation of blood lactate levels enhances flux through the glyceroneogenesis pathway, which increases the re-esterification rate of FA. Simulations demonstrate possible metabolic responses to altered expressions of PEPCK and ACS. Finally, a parameter sensitivity analysis indicates that insulin-stimulated glucose uptake could be severely affected by impairment of the GLUT4 translocation and glycolysis. Furthermore, reduced insulin action in these steps blunts the production of lactate by insulin.

Steady-state Analysis

Model simulations of the dependence of venous glycerol and rates of lipolysis and re-esterification of FA on insulin level correspond well to experimental data (Fig. 4). At the highest insulin level, the simulated glycerol level was ~35% higher than found experimentally. However, when the hydrolysis of plasma TG (i.e., VLDL-TG) by LPL was completely suppressed, simulated outputs and experimental data were in good agreement. This suggests that the discrepancy associated with high levels of venous glycerol and at the highest insulin level may be related to the breakdown of plasma TG by LPL rather than from the intracellular TG breakdown. Although our model has some limitations associated with the breakdown of plasma TG by LPL. It can simulate the lipolytic responses from intracellular lipolysis. In fact, plasma TG hydrolysis by LPL in the basal state accounts for only ~13% of the total TG breakdown in the adipose tissue from *in vivo*[10,14] and *in silico* studies.[21] Consequently, the effect of simulating LPL reaction was not evident in the basal state. However, the simulations in this study suggest that when the rate of lipolysis decreases more than 90% of the basal state, the breakdown of plasma TG by LPL can make a significant contribution to the total rate of TG breakdown in the adipose tissue. Therefore, simulating TG breakdown by LPL becomes critical when the intracellular lipolysis is suppressed by insulin.

Regulation of Lipolysis

Since the breakdown of TG and DG are catalyzed by different enzymes, viz., ATGL, HSL[42] and the first step in TG hydrolysis involves other regulatory proteins, such as perilipin A and adipophilin,[28,51] we hypothesized that TG and DG breakdowns are differentially suppressed by insulin. Therefore, the model parameters for these reactions were varied to simulate different insulin effects: differential suppression or no suppression of the ATGL reaction and uniform suppression of ATGL and HSL reactions. Insulin transcriptionally down-regulates the activity of ATGL.[20] Therefore, the effect of insulin on ATGL activity will be legible over the time scale of interest (~2 h). Instead, we assumed that insulin can suppress the breakdown of TG by ATGL indirectly by perilipin A since the inactivation of perilipin A limits the access of both ATGL and HSL to the TG stores, i.e., lipid droplets.[28] Model simulations predict the integrated responses that affect different regulation mechanisms.

The degree of suppression of ATGL did not affect the venous dynamics of glycerol since the production of glycerol depends on the hydrolysis of MG by HSL and MGL, which are not subject to the insulin mediated suppression. Simulations without suppressing ATGL reaction by insulin produced consistently higher levels of FA in the venous blood (Fig. 6b). Suppression by more than 50% did not further change venous FA concentration dynamics. This limits the evaluation of differential suppression of these intracellular lipolytic reactions based on blood measurements. However, differential activation of lipolytic reactions during epinephrine infusion could generate distinctive changes in lipolytic intermediates.[21] Thus, simulations were used to predict insulin responses of intracellular DG and MG concentrations. Whereas MG levels did not change, changes in DG could be distinguished. With uniform suppression of lipolytic reactions, DG continuously decreased with insulin; whereas with differential suppression of ATGL reaction, DG increased. If ATGL were not suppressed by insulin, then DG would increase more than 20%. Although corresponding data from *in vivo* experiments are not available, *in vitro* studies showed that insulin increases DG.[12] These studies used palmitate in the incubation medium. Therefore, the rate of DG synthesis was not limited by the availability of fatty acids. Without the infusion of fatty acids or the ingestion of mixed meal, the availability of fatty acids can limit the synthesis of DG and TG. Therefore, the accumulation of DG during hyperinsulinemic clamp experiment might be lower than that from *in vitro* studies. Model simulations, however,

indicate that DG levels may provide a clue to the mechanism by which insulin suppresses lipolytic reactions.

Glyceroneogenesis and PEPCK Over-expression

The metabolic importance of glyceroneogenesis in adipose tissue was examined previously by simulating responses to the increased rate of TG-FA cycle during epinephrine infusion.[21] However, there was no change in the rate of glucose uptake during intravenous epinephrine infusion. Therefore, the previous model could not determine the adipose tissue response to increased rate of glucose uptake. With our enhanced model, simulations showed that glycolytic and glyceroneogenic fluxes for G3P synthesis increased with stimulated glucose uptake. This may seem counter-intuitive because PEPCK, a regulatory enzyme for glyceroneogenesis, is down-regulated by insulin.[3] However, the transcriptional regulation of PEPCK by insulin requires a longer time to act than related to the time scale of acute experiments. Furthermore, the activity of PEPCK in the basal state in adipose tissue is high enough to meet the metabolic requirements. [34,35] Consequently, in acute response to insulin infusion the availability of substrates regulates the glyceroneogenic flux rather than a change in the activity of PEPCK *per se*.

Our simulations also show that in response to insulin, the total rate of G3P synthesis decreased with increasing direct glycolytic contribution in the basal state (Fig. 7b). GAP1, the precursor for G3P1 synthesis can also be used to produce pyruvate, which is activated by insulin. Thus, the direct glycolytic contribution to G3P synthesis is in competition with the entire glycolytic pathway such that the synthesis of G3P1 from GAP1 can be limited by insulin stimulated glycolysis. On the contrary, G3P2 synthesis via glyceroneogenesis has no such competition but requires more ATP and NADH. However, as shown in Fig. 7c, an increase in the rate of glycolytic flux by insulin decreased the redox state (C_{NAD^+}/C_{NADH}) and increased the phosphorylation state (C_{ATP}/C_{ADP}), thus increasing the driving force of the flux through glyceroneogenesis. Therefore, our model simulations indicate that glyceroneogenesis is more robust and significant pathway to synthesize G3P in response to insulin.

Glyceroneogenesis plays a significant role in regulating the synthesis of G3P (and therefore of TG). Thus, pyruvate and lactate are important as precursors. Indeed, increased insulin resistance with obesity has associated higher plasma and interstitial levels of lactate in the adipose tissue.[18,33] The effect of elevated plasma lactate on re-esterification of FA and glyceroneogenesis was analyzed by simulating experiments with elevated levels of arterial lactate. These simulations showed that FA re-esterification and flux through glyceroneogenesis increased 10–15%. Higher levels of lactate in plasma were associated with higher lactate levels in tissue. Since the cellular lactate levels affect the redox potential and pyruvate levels, the elevated lactate levels can promote the synthesis of G3P that increases intracellular FA re-esterification.

Simulated responses from the altered PEPCK expression were obtained by changing the maximum reaction rate coefficient for the reaction catalyzed by PEPCK. Even though the activity of PEPCK increased the flux through glyceroneogenesis, the FA release rate into circulation did not decrease. These simulations indicate that synthesis of FAC from FA by ACS should increase together with PEPCK activity to increase the rate of FA re-esterification as measured in the transgenic animals.[13] Decreased FA release rate from adipose tissue was also observed by the treatment of diabetic subjects with TZDs.[52] Since TZDs are PPARγ agonists, they can affect several metabolic pathways involved in glucose and fatty acids homeostasis. *In vivo* studies showed that the PPARγ treatment upregulated the genes for PEPCK and ACS in the adipose tissue.[26,53] Simulations were consistent with these observations as indicated by increases in enzyme activities and flux rates. These

simulations indicate that the upregulation of PEPCK *per se* is not sufficient to increase the rate of FA re-esterification and are expected to be accompanied by the induction of other enzymes, specifically, ACS.

Effect of Impaired Insulin Action

Insulin resistance is a state of tissue or whole body requiring higher levels of insulin to elicit a normal response.[49] The decreased rate of insulin-stimulated glucose uptake is one of the major defects resulted from insulin resistance. This effect was simulated by decreasing the model parameter values related to stimulatory insulin action. Impairments in GLUT4 translocation and glycolysis including phosphorylation of glucose had more significant effect on the rate of glucose uptake by the adipose tissue than changes in rates of glycogen synthesis and pyruvate oxidation. This indicates that glucose transport and subsequent phosphorylation are the principal sites of defective insulin action in the adipose tissue. Indeed, various *in vivo* studies in skeletal muscle showed that the stimulation of GLUT4 translocation and phosphorylation of glucose were the primary impairments in type 2 diabetes.[38,44] Even though the rate of glycogen synthesis was impaired in these patients, it was secondary to the defects in glucose transport and phosphorylation.

In vivo studies in humans showed that the insulin-resistant obese subjects in the basal state had an elevated lactate release, which did not increase in response to insulin infusion.[33] In contrast, normal lean subjects showed an increase of lactate release rate during the hyperinsulinemic-euglycemic clamp experiment. [33] By decreasing model parameters values associated with GLUT4 translocation and glycolysis, the rate of lactate release decreased. When the parameter decreases are sufficiently large, the lactate release rate returned to the basal state as reported from *in vivo* studies in obese subjects. The opposite response occurred with the impaired glycogen synthesis and pyruvate oxidation. One explanation is that glycogen synthesis and pyruvate oxidation are not the predominant mechanisms of consumption of glucose taken up by the adipose tissue. More than 70% of glucose taken up by the skeletal muscle is converted to glycogen during hyperinsulinemic-euglycemic clamp.[11,43] In contrast, in the adipose tissue, model simulations showed that only ~30% of glucose uptake was used for this purpose. More glucose is used to produce lactate in adipose tissue than in skeletal muscle. This indicates the relative importance of lactate production for insulin-stimulated glucose disposal in the adipose tissue. Consistent with experimental data, model simulations show that the pathways for defective insulin action play an important role in the adipose tissue and that insulin resistance is associated with the decreased translocation of glucose transporters and glycolysis in adipose tissue.

Model Limitations

One limitation of our enhanced computational model of adipose tissue metabolism is incomplete suppression of plasma TG breakdown in response to insulin, which depends on the breakdown of TG by LPL in the blood compartment. From *in vivo* human studies,[9] plasma levels of TG slowly decreased by ~ 20% in response to insulin. Since the reaction flux of TG hydrolysis by LPL in the enhanced model depends on the total plasma level of TG, the plasma TG breakdown rate cannot decrease to a negligible level found with *in vivo* studies.[9] LPL may have different affinity toward various lipoproteins (e.g., VLDL, chylomicrons, LDL *etc.*). Indeed, chylomicrons have more than a 50-fold higher affinities toward LPL.[54] Furthermore, the size distribution of plasma VLDL shifts toward a smaller size during a hyperinsulinemic clamp experiment.[22] Therefore, LPL might have lower specific affinity toward TG-depleted small VLDL. Future studies should consider varying activities of LPL for different lipoproteins to describe the regulation of plasma TG breakdown.

CONCLUSIONS

An enhanced mechanistic, computational model of adipose tissue metabolism *in vivo* simulated steady-state responses to insulin as well as dynamic changes in venous concentrations of metabolites during the hyperinsulinemic-euglycemic clamp experiment. Our simulations studies indicate that the regulation of LPL becomes important when intracellular lipolysis is suppressed by insulin. Different activities of LPL toward various lipoproteins should be considered to investigate the regulation of lipolysis in the adipose tissue. Differential suppression of lipolytic reactions by insulin is required to increase the levels of DG as measured *in vitro* studies. Model simulations indicate that glyceroneogenesis is the dominant pathway for G3P synthesis even when the rate of glucose uptake is increased. Simulations of the effect of altered enzyme expression showed that the increased rate of re-esterification requires the upregulation of both PEPCK and ACS activities. This demonstrates the usefulness of this model in predicting phenotypic responses resulted from genetic modulations. Finally, simulations are consistent with studies showing that in the primary metabolic pathways of insulin-resistant adipose tissue, the main defects are associated with GLUT4 translocation and glycolysis (i.e., phosphorylation).

Acknowledgments

This research was supported by a grant (P50-GM-66309) from the National Institute of General Medical Sciences for developing a Center for Modeling Integrated Metabolic Systems at Case Western Reserve University.

References

1. Assimacopoulos-Jeannet F, Jeanrenaud B. Insulin activates 6-phosphofructo-2-kinase and pyruvate kinase in the liver. Indirect evidence for an action via a phosphatase. J Biol Chem. 1990; 265:7202–7206. [PubMed: 2158992]
2. Assimacopoulos-Jeannet F, Cusin I, Greco-Perotto RM, Terrettaz J, Rohner-Jeanrenaud F, Zarjevski N, Jeanrenaud B. Glucose transporters: structure, function, and regulation. Biochimie. 1991; 73:67–70. [PubMed: 2031959]
3. Beale EG, Tishler EJ. Expression and regulation of cytosolic phosphoenolpyruvate carboxykinase in 3T3-L1 adipocytes. Biochem Biophys Res Commun. 1992; 189:925–930. [PubMed: 1335249]
4. Bodenlenz M, Schaupp LA, Druml T, Sommer R, Wutte A, Schaller HC, Sinner F, Wach P, Pieber TR. Measurement of interstitial insulin in human adipose and muscle tissue under moderate hyperinsulinemia by means of direct interstitial access. Am J Physiol Endocrinol Metab. 2005; 289:E296–E300. [PubMed: 15769794]
5. Carmen GY, Victor SM. Signalling mechanisms regulating lipolysis. Cell Signal. 2006; 18:401–408. [PubMed: 16182514]
6. Casazza JP, Veech RL. The interdependence of glycolytic and pentose cycle intermediates in ad libitum fed rats. J Biol Chem. 1986; 261:690–698. [PubMed: 3079759]
7. Chang TJ, Lee WJ, Chang HM, Lee KC, Chuang LM. Expression of subcutaneous adipose tissue phosphoenolpyruvate carboxykinase correlates with body mass index in nondiabetic women. Metabolism. 2008; 57:367–372. [PubMed: 18249209]
8. Coppack SW, Frayn KN, Humphreys SM, Dhar H, Hockaday TD. Effects of insulin on human adipose tissue metabolism in vivo. Clin Sci (Lond). 1989; 77:663–670. [PubMed: 2691176]
9. Coppack SW, Frayn KN, Humphreys SM. Plasma triacylglycerol extraction in human adipose tissue in vivo: effects of glucose ingestion and insulin infusion. Eur J Clin Nutr. 1989; 43:493–496. [PubMed: 2680476]
10. Coppack SW, Frayn KN, Humphreys SM, Whyte PL, Hockaday TD. Arteriovenous differences across human adipose and forearm tissues after overnight fast. Metabolism. 1990; 39:384–390. [PubMed: 2109165]

11. DeFronzo RA, Jacot E, Jequier E, Maeder E, Wahren J, Felber JP. The effect of insulin on the disposal of intravenous glucose. Results from indirect calorimetry and hepatic and femoral venous catheterization. Diabetes. 1981; 30:1000–1007. [PubMed: 7030826]
12. Edens NK, Leibel RL, Hirsch J. Lipolytic effects on diacylglycerol accumulation in human adipose tissue in vitro. J Lipid Res. 1990; 31:1351–1359. [PubMed: 2280178]
13. Franckhauser S, Munoz S, Pujol A, Casellas A, Riu E, Otaegui P, Su B, Bosch F. Increased fatty acid re-esterification by PEPCK overexpression in adipose tissue leads to obesity without insulin resistance. Diabetes. 2002; 51:624–630. [PubMed: 11872659]
14. Frayn KN, Shadid S, Hamlani R, Humphreys SM, Clark ML, Fielding BA, Boland O, Coppack SW. Regulation of fatty acid movement in human adipose tissue in the postabsorptive-to-postprandial transition. Am J Physiol. 1994; 266:E308–E317. [PubMed: 8166251]
15. Grimmsmann T, Levin K, Meyer MM, Beck-Nielsen H, Klein HH. Delays in insulin signaling towards glucose disposal in human skeletal muscle. J Endocrinol. 2002; 172:645–651. [PubMed: 11874713]
16. Haemmerle G, Zimmermann R, Hayn M, Theussl C, Waeg G, Wagner E, Sattler W, Magin TM, Wagner EF, Zechner R. Hormone-sensitive lipase deficiency in mice causes diglyceride accumulation in adipose tissue, muscle, and testis. J Biol Chem. 2002; 277:4806–4815. [PubMed: 11717312]
17. Haemmerle G, Lass A, Zimmermann R, Gorkiewicz G, Meyer C, Rozman J, Heldmaier G, Maier R, Theussl C, Eder S, Kratky D, Wagner EF, Klingenspor M, Hoefler G, Zechner R. Defective lipolysis and altered energy metabolism in mice lacking adipose triglyceride lipase. Science. 2006; 312:734–737. [PubMed: 16675698]
18. Jansson PA, Larsson A, Smith U, Lonnroth P. Lactate release from the subcutaneous tissue in lean and obese men. J Clin Invest. 1994; 93:240–246. [PubMed: 8282793]
19. Karpe F, Fielding BA, Ardilouze JL, Ilic V, Macdonald IA, Frayn KN. Effects of insulin on adipose tissue blood flow in man. J Physiol. 2002; 540:1087–1093. [PubMed: 11986393]
20. Kershaw EE, Hamm JK, Verhagen LA, Peroni O, Katic M, Flier JS. Adipose triglyceride lipase: function, regulation by insulin, and comparison with adiponutrin. Diabetes. 2006; 55:148–157. [PubMed: 16380488]
21. Kim J, Saidel GM, Kalhan SC. A computational model of adipose tissue metabolism: evidence for intracellular compartmentation and differential activation of lipases. J Theor Biol. 2008; 251:523–540. [PubMed: 18234232]
22. Lewis GF, Uffelman KD, Szeto LW, Steiner G. Effects of acute hyperinsulinemia on VLDL triglyceride and VLDL apoB production in normal weight and obese individuals. Diabetes. 1993; 42:833–842. [PubMed: 8495807]
23. Londos C, Brasaemle DL, Schultz CJ, Segrest JP, Kimmel AR. Perilipins, ADRP, and other proteins that associate with intracellular neutral lipid droplets in animal cells. Semin Cell Dev Biol. 1999; 10:51–58. [PubMed: 10355028]
24. Mandarino LJ, Consoli A, Jain A, Kelley DE. Differential regulation of intracellular glucose metabolism by glucose and insulin in human muscle. Am J Physiol. 1993; 265:E898–E905. [PubMed: 8279545]
25. Mandarino LJ, Printz RL, Cusi KA, Kinchington P, O'Doherty RM, Osawa H, Sewell C, Consoli A, Granner DK, DeFronzo RA. Regulation of hexokinase II and glycogen synthase mRNA, protein, and activity in human muscle. Am J Physiol. 1995; 269:E701–E708. [PubMed: 7485484]
26. Martin G, Schoonjans K, Lefebvre AM, Staels B, Auwerx J. Coordinate regulation of the expression of the fatty acid transport protein and acyl-CoA synthetase genes by PPARalpha and PPARgamma activators. J Biol Chem. 1997; 272:28210–28217. [PubMed: 9353271]
27. McLean P, Greenbaum AL, Brown J, Greenslade KR. Influence of hormones on the nicotinamide nucleotide coenzymes of adipose tissue. Biochem J. 1967; 105:1013–1018. [PubMed: 16742525]
28. Miyoshi H, Perfield JW, Souza SC, Shen WJ, Zhang HH, Stancheva ZS, Kraemer FB, Obin MS, Greenberg AS. Control of adipose triglyceride lipase action by serine 517 of perilipin A globally regulates protein kinase A-stimulated lipolysis in adipocytes. J Biol Chem. 2007; 282:996–1002. [PubMed: 17114792]

29. Moustaid N, Jones BH, Taylor JW. Insulin increases lipogenic enzyme activity in human adipocytes in primary culture. J Nutr. 1996; 126:865–870. [PubMed: 8613889]
30. Muretta JM, Romenskaia I, Mastick CC. Insulin releases Glut4 from static storage compartments into cycling endosomes and increases the rate constant for Glut4 exocytosis. J Biol Chem. 2008; 283:311–323. [PubMed: 17967900]
31. Nye CK, Hanson RW, Kalhan SC. Glyceroneogenesis is the dominant pathway for triglyceride glycerol synthesis in vivo in the rat. J Biol Chem. 2008; 283:27565–27574. [PubMed: 18662986]
32. Pastan I, Wills V, Herring B, Field JB. Pyridine nucleotides in the thyroid. I. A method for the measurement of oxidized and reduced triphosphopyridine nucleotides with the use of 6-Pphosphogluconate-1-C14. J Biol Chem. 1963; 238:3362–3365. [PubMed: 14085387]
33. Qvisth V, Hagstrom-Toft E, Moberg E, Sjoberg S, Bolinder J. Lactate release from adipose tissue and skeletal muscle in vivo: defective insulin regulation in insulin-resistant obese women. Am J Physiol Endocrinol Metab. 2007; 292:E709–E714. [PubMed: 17077346]
34. Reshef L, Hanson RW. The interaction of catecholamines and adrenal corticosteroids in the induction of phosphopyruvate carboxylase in rat liver and adipose tissue. Biochem J. 1972; 127:809–818. [PubMed: 4342497]
35. Reshef L, Hanson RW, Ballard FJ. Glyceride-glycerol synthesis from pyruvate. Adaptive changes in phosphoenolpyruvate carboxykinase and pyruvate carboxylase in adipose tissue and liver. J Biol Chem. 1969; 244:1994–2001. [PubMed: 5781996]
36. Reshef L, Olswang Y, Cassuto H, Blum B, Croniger CM, Kalhan SC, Tilghman SM, Hanson RW. Glyceroneogenesis and the triglyceride/fatty acid cycle. J Biol Chem. 2003; 278:30413–30416. [PubMed: 12788931]
37. Rigden DJ, Jellyman AE, Frayn KN, Coppack SW. Human adipose tissue glycogen levels and responses to carbohydrate feeding. Eur J Clin Nutr. 1990; 44:689–692. [PubMed: 2261901]
38. Rothman DL, Shulman RG, Shulman GI. 31P nuclear magnetic resonance measurements of muscle glucose-6-phosphate. Evidence for reduced insulin-dependent muscle glucose transport or phosphorylation activity in non-insulin-dependent diabetes mellitus. J Clin Invest. 1992; 89:1069–1075. [PubMed: 1556176]
39. Sadiq F, Hazlerigg DG, Lomax MA. Amino acids and insulin act additively to regulate components of the ubiquitin-proteasome pathway in C2C12 myotubes. BMC Mol Biol. 2007; 8:23. [PubMed: 17371596]
40. Saggerson ED, Greenbaum AL. The regulation of triglyceride synthesis and fatty acid synthesis in rat epididymal adipose tissue. Biochem J. 1970; 119:193–219. [PubMed: 4395181]
41. Samra JS, Simpson EJ, Clark ML, Forster CD, Humphreys SM, Macdonald IA, Frayn KN. Effects of epinephrine infusion on adipose tissue: interactions between blood flow and lipid metabolism. Am J Physiol. 1996; 271:E834–E839. [PubMed: 8944669]
42. Schweiger M, Schreiber R, Haemmerle G, Lass A, Fledelius C, Jacobsen P, Tornqvist H, Zechner R, Zimmermann R. Adipose triglyceride lipase and hormone-sensitive lipase are the major enzymes in adipose tissue triacylglycerol catabolism. J Biol Chem. 2006; 281:40236–40241. [PubMed: 17074755]
43. Serlie MJ, de Haan JH, Tack CJ, Verberne HJ, Ackermans MT, Heerschap A, Sauerwein HP. Glycogen synthesis in human gastrocnemius muscle is not representative of whole-body muscle glycogen synthesis. Diabetes. 2005; 54:1277–1282. [PubMed: 15855310]
44. Shulman RG, Rothman DL. Enzymatic phosphorylation of muscle glycogen synthase: a mechanism for maintenance of metabolic homeostasis. Proc Natl Acad Sci USA. 1996; 93:7491–7495. [PubMed: 8755501]
45. Staples J, Suarez R. Honeybee flight muscle phosphoglucose isomerase: matching enzyme capacities to flux requirements at a near-equilibrium reaction. J Exp Biol. 1997; 200:1247–1254. [PubMed: 9319107]
46. Stralfors P, Honnor RC. Insulin-induced dephosphorylation of hormone-sensitive lipase. Correlation with lipolysis and cAMP-dependent protein kinase activity. Eur J Biochem. 1989; 182:379–385. [PubMed: 2661229]

47. Strawford A, Antelo F, Christiansen M, Hellerstein MK. Adipose tissue triglyceride turnover, de novo lipogenesis, and cell proliferation in humans measured with 2H2O. Am J Physiol Endocrinol Metab. 2004; 286:E577–E588. [PubMed: 14600072]
48. Stumvoll M, Jacob S, Wahl HG, Hauer B, Loblein K, Grauer P, Becker R, Nielsen M, Renn W, Haring H. Suppression of systemic, intramuscular, and subcutaneous adipose tissue lipolysis by insulin in humans. J Clin Endocrinol Metab. 2000; 85:3740–3745. [PubMed: 11061533]
49. Summers LK. Adipose tissue metabolism, diabetes and vascular disease—lessons from in vivo studies. Diab Vasc Dis Res. 2006; 3:12–21. [PubMed: 16784176]
50. Syed NA, Khandelwal RL. Reciprocal regulation of glycogen phosphorylase and glycogen synthase by insulin involving phosphatidylinositol-3 kinase and protein phosphatase-1 in HepG2 cells. Mol Cell Biochem. 2000; 211:123–136. [PubMed: 11055555]
51. Sztalryd C, Xu G, Dorward H, Tansey JT, Contreras JA, Kimmel AR, Londos C. Perilipin A is essential for the translocation of hormone-sensitive lipase during lipolytic activation. J Cell Biol. 2003; 161:1093–1103. [PubMed: 12810697]
52. Tordjman J, Chauvet G, Quette J, Beale EG, Forest C, Antoine B. Thiazolidinediones block fatty acid release by inducing glyceroneogenesis in fat cells. J Biol Chem. 2003; 278:18785–18790. [PubMed: 12644461]
53. Way JM, Harrington WW, Brown KK, Gottschalk WK, Sundseth SS, Mansfield TA, Ramachandran RK, Willson TM, Kliewer SA. Comprehensive messenger ribonucleic acid profiling reveals that peroxisome proliferator-activated receptor gamma activation has coordinate effects on gene expression in multiple insulin-sensitive tissues. Endocrinology. 2001; 142:1269–1277. [PubMed: 11181544]
54. Xiang SQ, Cianflone K, Kalant D, Sniderman AD. Differential binding of triglyceride-rich lipoproteins to lipoprotein lipase. J Lipid Res. 1999; 40:1655–1663. [PubMed: 10484612]
55. Yang YJ I, Hope D, Ader M, Bergman RN. Insulin transport across capillaries is rate limiting for insulin action in dogs. J Clin Invest. 1989; 84:1620–1628. [PubMed: 2681272]

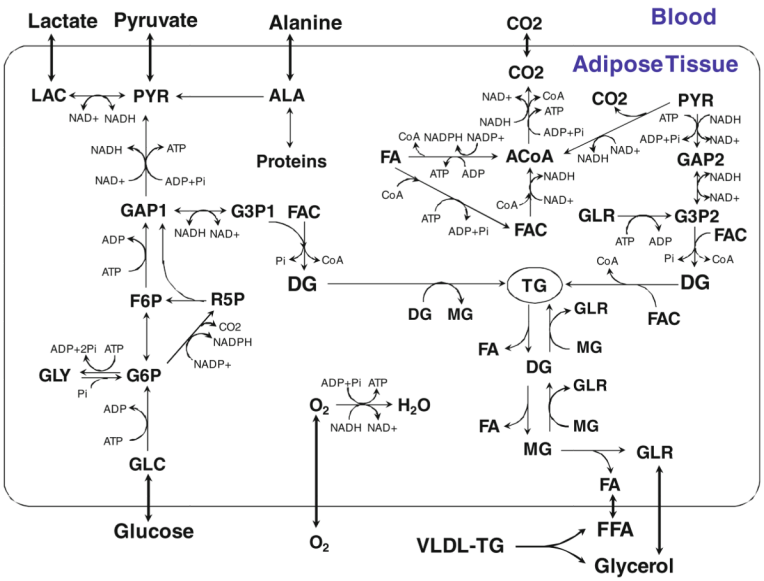

FIGURE 1.

Metabolic pathways in the adipose tissue. The model incorporates various metabolic pathways including glycolysis, glycogen cycle, pentose phosphate shunt, pyruvate oxidation, beta-oxidation, tricarboxylic acid cycle, oxidative phosphorylation, proteolysis and the esterification and hydrolysis of triglycerides. Glycerol-3-phosphate (G3P), used for the esterification of fatty acids, is formed either from glucose via glycolysis or from pyruvate via glyceroneogenesis. Triose phosphates (GAP, G3P) are heterogeneously distributed in the cellular compartment. GAP1 and G3P1 represent the triose phosphate pool from glycolysis, whereas GAP2 and G3P2 represent the pool from glyceroneogenesis. The arrow with both ends indicates a reversible reaction step. GLC, glucose; PYR, pyruvate; LAC, lactate; ALA, alanine; GLR, glycerol; FA, fatty acids; GLY, glycogen; G6P, glucose-6-phosphate; F6P, fructose-6-phosphate; R5P, ribulose-5-phosphate; GAP, glyceraldehyde-3-phasphate; G3P, glycerol-3-phosphate; ACoA, acetyl CoA; FAC, fatty acyl CoA; TG, triglycerides; DG, diglycerides; MG, monoglycerides.

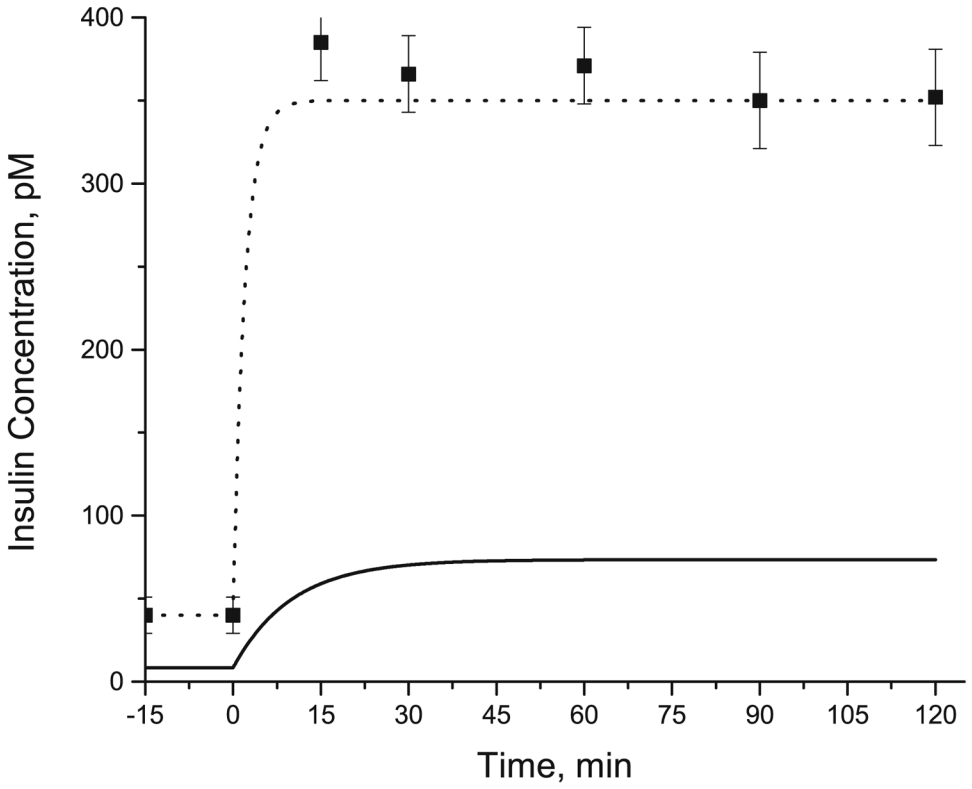

FIGURE 2.

Dynamic changes in the plasma and interstitial concentrations of insulin following a constant rate intravenous infusion of insulin at 0 min. Assuming a step increase in the plasma levels of insulin (dotted line), the corresponding levels of insulin in the interstitial fluid (solid line) was simulated assuming a time constant of 10 min. Square symbol represents the plasma levels of insulin from the experimental studies in human.[8]

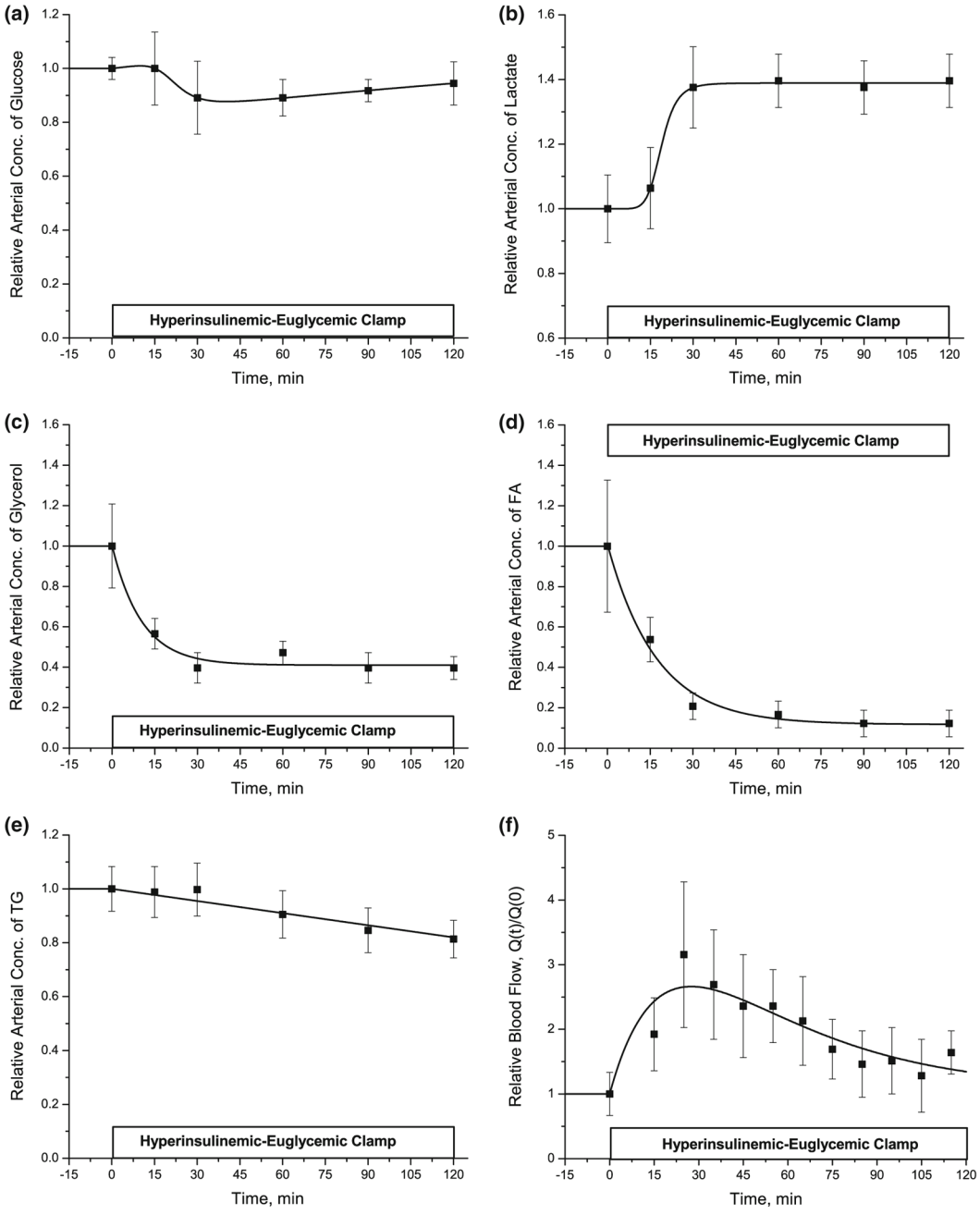

FIGURE 3.

Dynamic changes in the arterial concentrations of glucose (a), lactate (b), glycerol (c), FA (d) and TG (e), and the adipose blood flow (f) during hyperinsulinemic-euglycemic clamp. Relative concentration/blood flow is the ratio of concentration/ blood flow at any time $t>0$ to $t = 0$. Squares represent the experimental data (mean ± SEM) from the references [8,9,19]. Solid lines are model simulations.

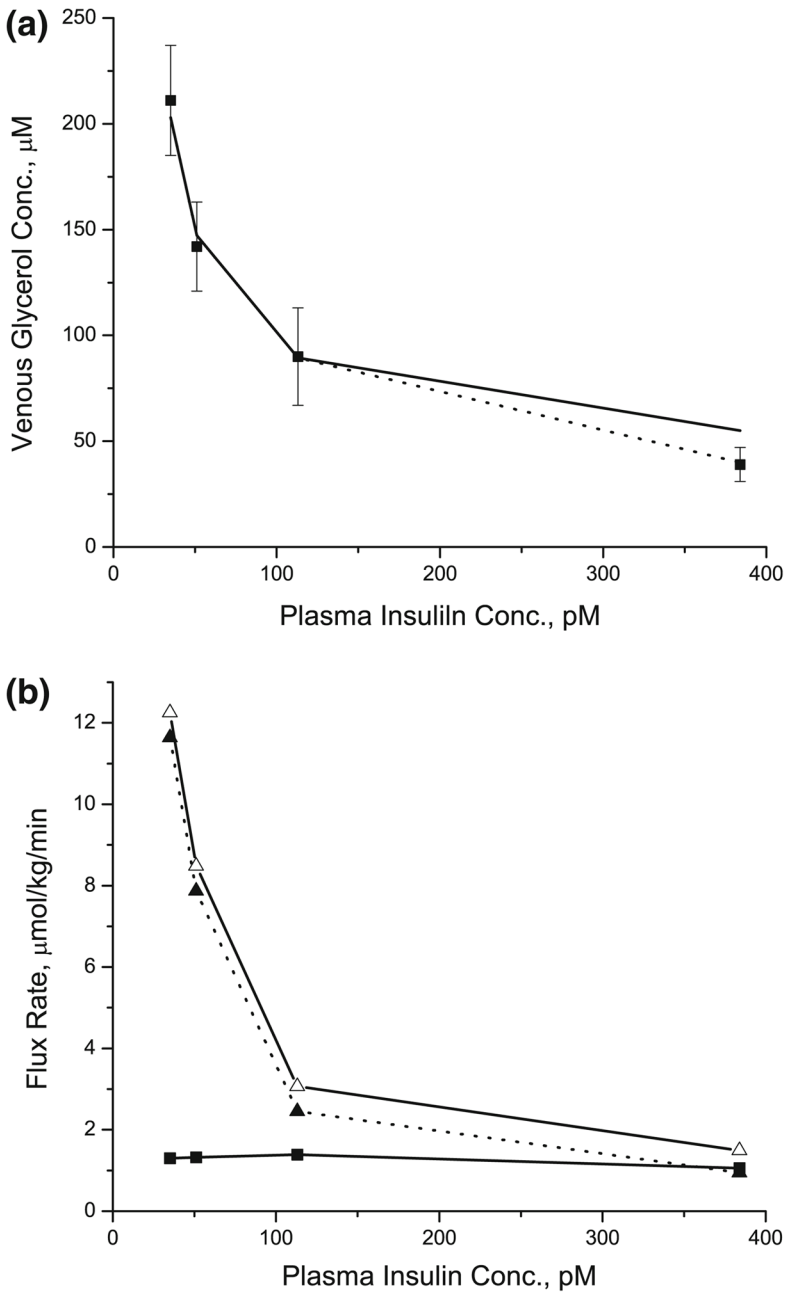

FIGURE 4.

Steady state insulin dose-responses for the venous glycerol concentrations and the rates of lipolysis and re-esterification. (a) Filled square symbol represents the experimental data from the reference [48]. Solid and dotted line represent the model simulations with (dotted line) or without (solid line) the complete suppression of plasma TG breakdown by LPL at the plasma insulin concentration of 383 pM. (b) While open triangle with solid line represents the rate of total lipolysis in the blood and cellular compartments, filled triangle with dotted line represents the rate of intracellular lipolysis. Filled square with solid line represents the rate of re-esterification of FA.

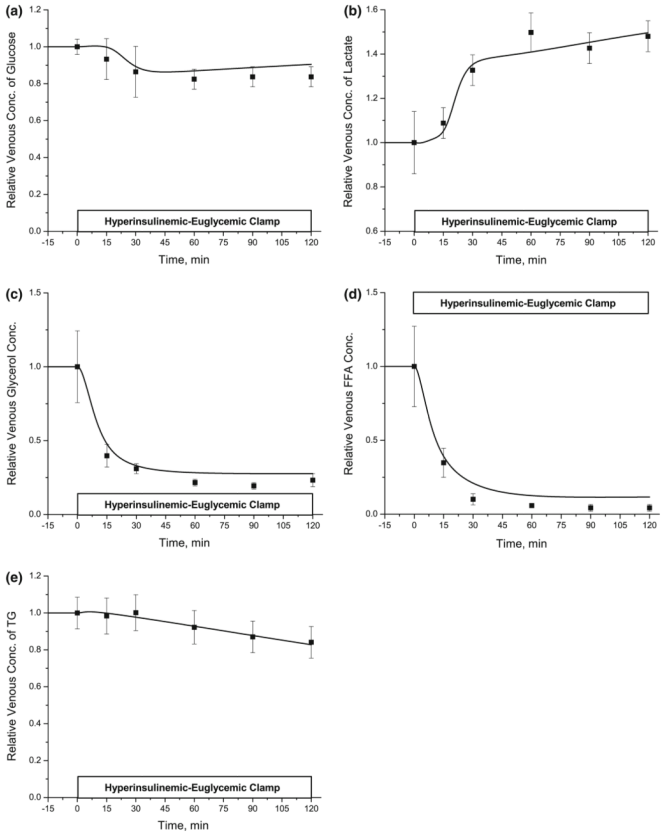

FIGURE 5.

Dynamic changes in the venous concentrations of glucose (a), lactate (b), glycerol (c), FA (d) and TG (e) in the adipose tissue during hyperinsulinemic-euclycemic clamp. Relative concentration is the ratio at any time $t>0$ to $t = 0$. Squares represent the experimental data (mean ± SEM) from the references [8,9]. Solid lines are model simulations.

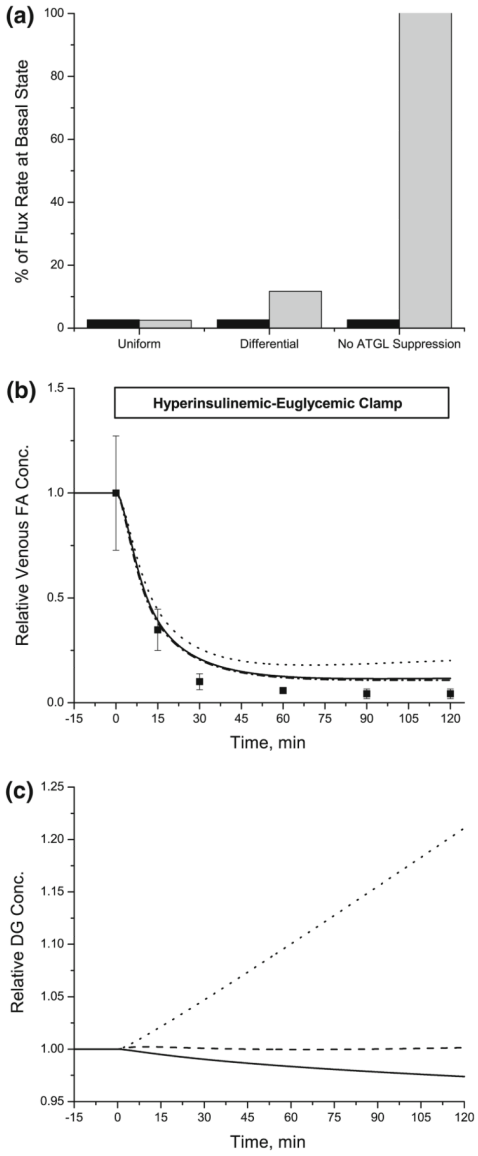

FIGURE 6.

Effect of differential suppression of lipolytic reactions on the venous concentration dynamics of FA and the changes in the levels of DG. (a): Relative changes in the flux rate of TG breakdown by ATGL (light gray bar) and TG and DG breakdowns by HSL (black bar) as a result of modulating the model parameter, $a_{TG \rightarrow DG,ATGL}$. The different values of $a_{TG \rightarrow DG,ATGL}$were used for "Uniform$a_{TG \rightarrow DG,ATGL}$ = 70.6 pM^2)" and "Differential ($a_{TG \rightarrow DG,ATGL}$ = 635 pM^2)". $V_{max,\ TG \rightarrow DG,ATGL}$ was not modulated by insulin in case of "No ATGL suppression". (b), (c): Dynamic changes in the relative venous concentrations of FA (b) and the relative intracellaur concentrations of DG (c). Relative concentration is the ratio of concentration at any time $t>0$ to $t = 0$. Squares represent the experimental data (mean ± SEM) from the references.[8] Model simulations (solid line: "Uniform", dashed line: "Differential" and dotted line: "No ATGL suppression) were based on the different values of $a_{TG \rightarrow DG,ATGL}$ as mentioned in (a).

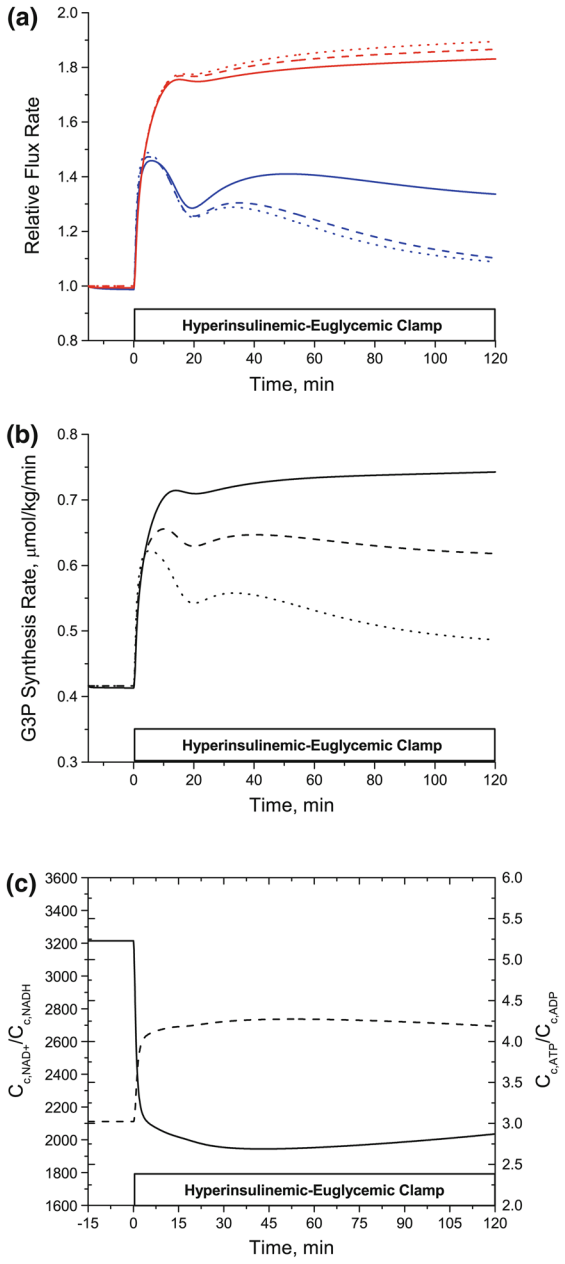

FIGURE 7.

(a) Relative changes in the rate of G3P synthesis via direct glycolysis and glyceroneogenesis (b) Dynamic changes in the rate of total G3P synthesis (c) Cellular phosphorylation and redox states. (a) Model simulations representing the relative changes in the rate of G3P synthesis via glyceroneogenesis (red line) and via direct glycolysis (blue line). Solid, dashed and dotted lines indicate the different ratios of glyceroneogenesis and direct glycolysis in the basal state. The ratios of glyceroneogenesis to direct glycolysis used in the model simulations were 10:1 (solid line), 1:1 (dashed line) and 1:10 (dotted line). (b) Relative flux rate (ratio of flux at time t>0 to that at t = 0). Solid, dashed and dotted lines are the changes in the rate of total G3P synthesis with different ratios of glyceroneogenesis to direct glycolysis. (c): Changes in the cellular redox (solid line, $C_{c,NAD^+}/C_{c,NADH}$) and phosphorylation (dashed line, $C_{c,ATP}/C_{c,ADP}$) states.

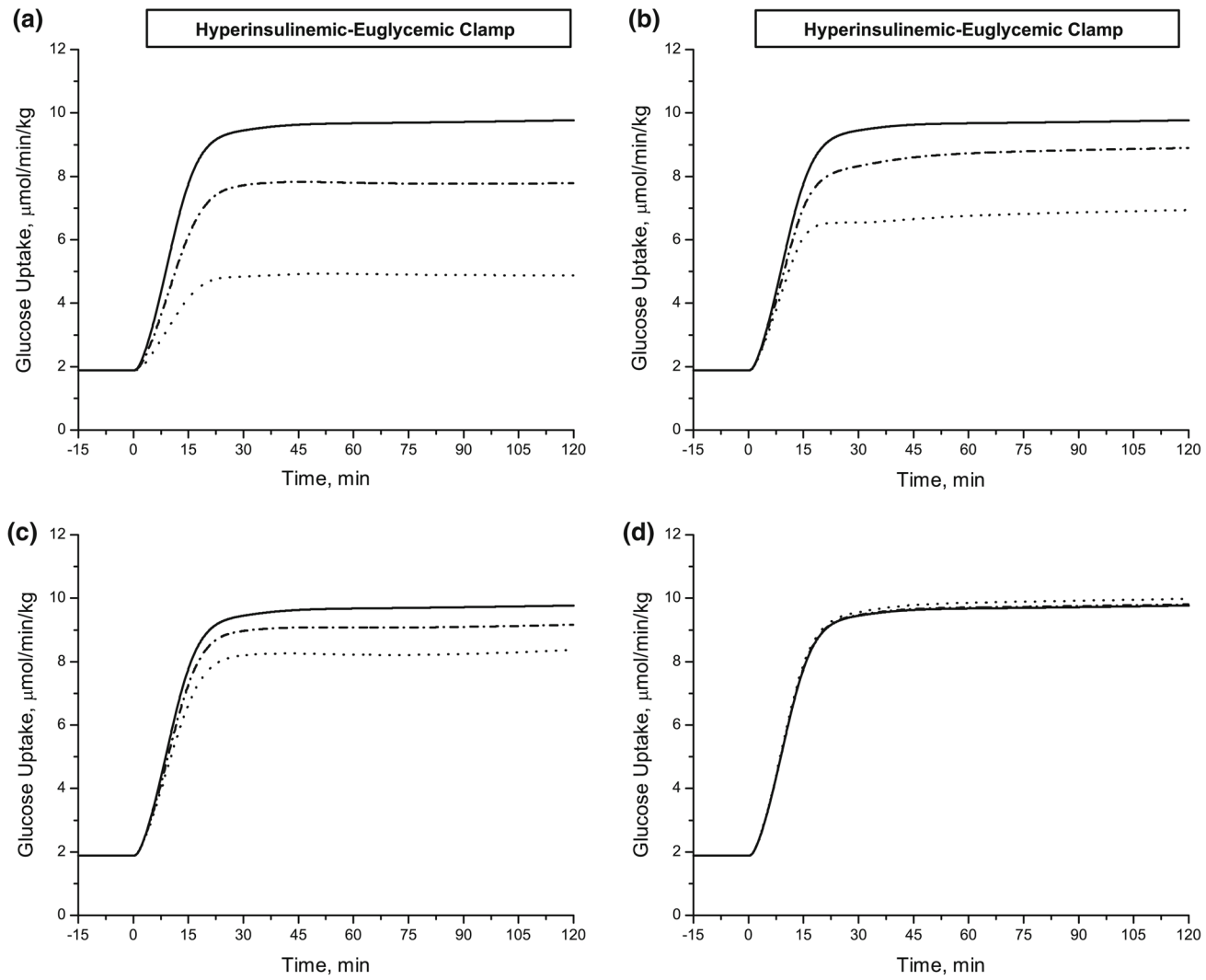

FIGURE 8.

Effect of defective insulin action on the rate of glucose uptake. The model predicted the changes in the rate of glucose uptake during hyperinsulinemic-euglycemic clamp as a result of varying the model parameters related to the stimulated insulin action; (a) $\lambda_{\text{Glycolysis}}$, (b) $\lambda_{\text{Tmax,GLC}}$, (c) $\lambda_{\text{Glycogen Synthesis}}$ and (d) λ_{PDH}. The parameters are decreased up to 20% of their estimated values in Table 5; Solid line (100% of estimated value, no change), dash-dotted line (60% of estimated value) and dotted line (20% of estimated value).

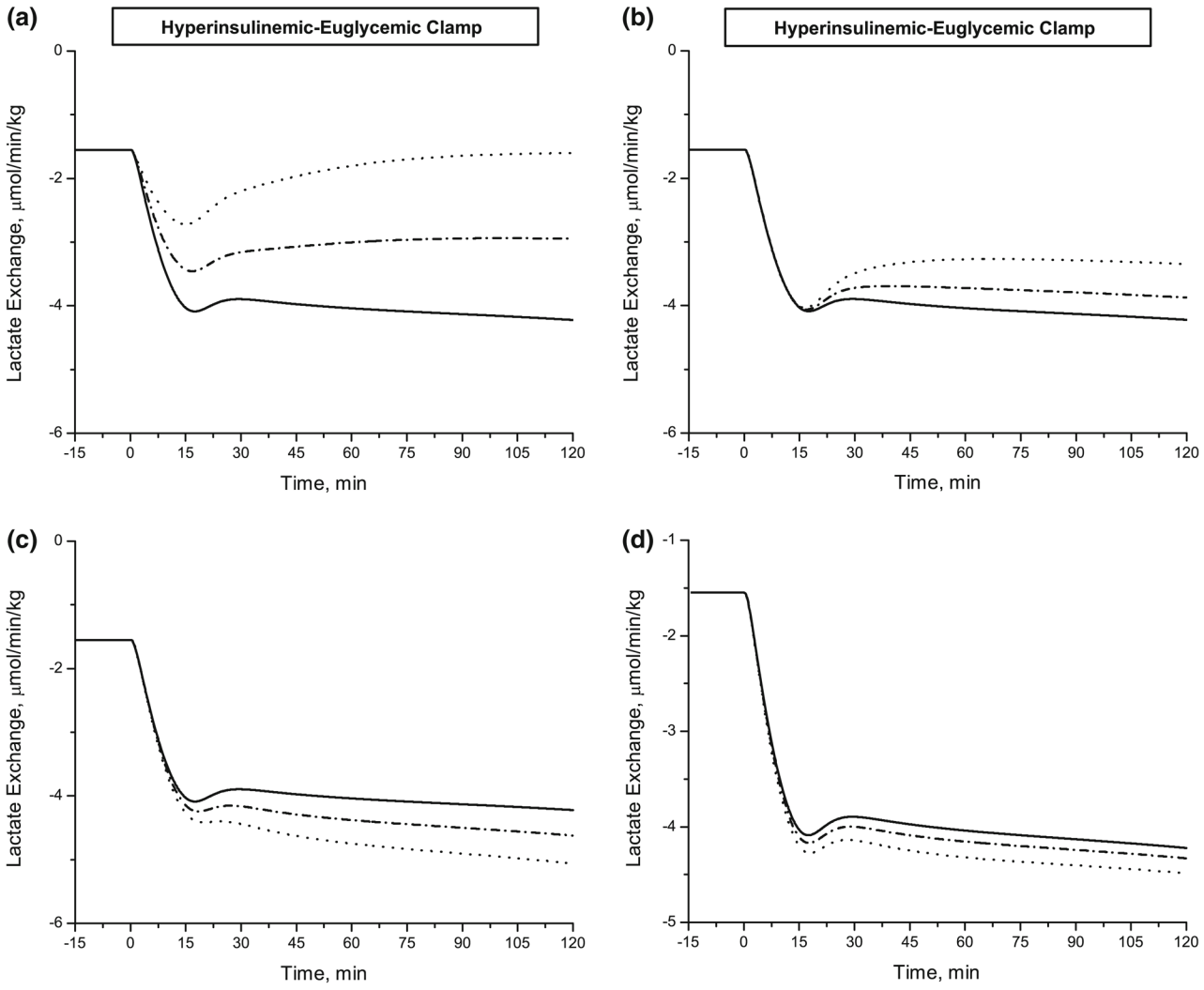

FIGURE 9.

Effect of defective insulin action on lactate exchange rate. A Model prediction of changes in lactate exchange rate during hyperinsulinemic-euglycemic clamp. Defining the lactate exchange rate defined as $Q \cdot (C_{\mathrm{a,LAC}} - C_{\mathrm{v,LAC}})$ leads to a negative net release of lactate from adipose tissue. Parameter values related to stimulated insulin action: (a) $\lambda_{\mathrm{Glycolysis}}$, (b) $\lambda_{T_{\mathrm{max,GLC}}}$, (c) $\lambda_{\mathrm{Glycogen\ Synthesis}}$ and (d) λ_{PDH}. The parameters are decreased up to 60% of their estimated values in Table 5; Solid line (100% of estimated value, no change), dash-dotted line (80% of estimated value) and dotted line (60% of estimated value).

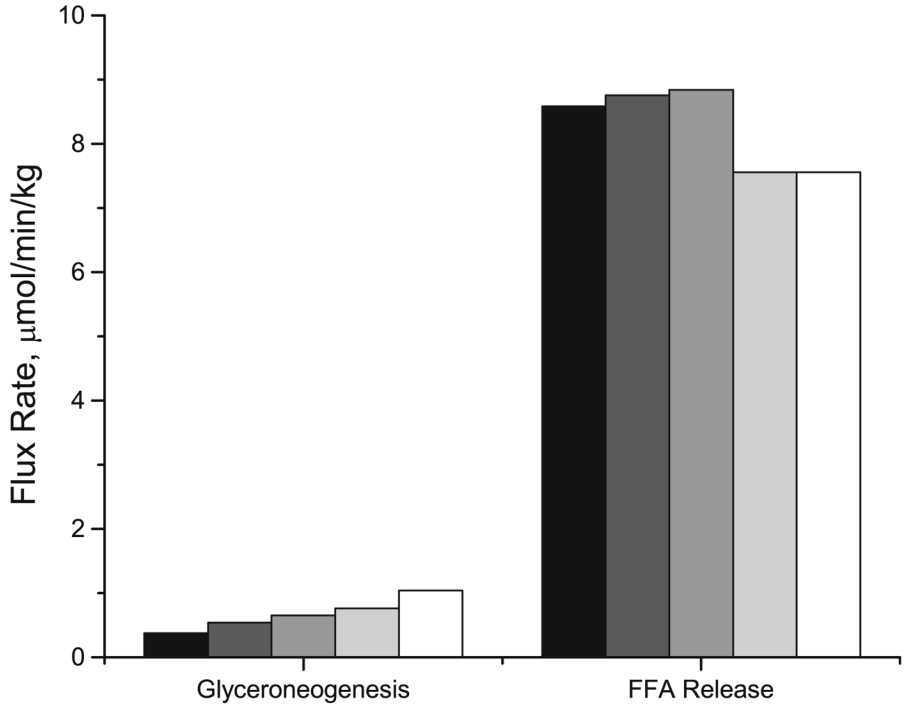

FIGURE 10.

Effect of altered enzyme activity on the rates of glyceroneogenesis and FA release. Control (black bar) is the model simulations with the maximum rate coefficients for PEPCK and ACS in the basal state ($V_{max,PEPCK}$ and $V_{max,ACS}$). For other simulations, $V_{max,PEPCK}$ increased two to three fold with or without two fold increase in $V_{max,ACS}$; Dark gray bar: 2 * $V_{max,PEPCK}$ and $V_{max,ACS}$; Gray bar: 3 * $V_{max,PEPCK}$ and $V_{max,ACS}$; Light gray bar: 2 * $V_{max,PEPCK}$ and 2 * $V_{max,ACS}$; Open bar: 3 * $V_{max,PEPCK}$ and 2 * $V_{max,ACS}$.

TABLE 1

Substrate concentration in the blood and the cellular compartment*.

Substrate	Blood	Cell
GLC	5000	2540
PYR	68	200
LAC	700	1440
ALA	192	1300
GLR	70	220
FA	660	1000
TG	990	990,000
O_2 (Total)	8000	34
O_2 (Free)	84	
CO_2 (Total)	21,700	15,427
CO_2 (Free)	1124	1403
GLY		13,000 [37]
G6P		210 [40]
F6P		60 [40]
GAP1, GAP2		10
G3P1, G3P2		150 [40]
R5P		4 [6]
ACoA		25
FAC		70 [40]
CoA		200
DG		2000
MG		200
ATP		3840 [40]
ADP		1270 [40]
Pi		2700
NAD^+		450 [40]
NADH		0.14 [40]
$NADP^+$		0.93 [27,32]
NADPH		7.1 [27,32]

*Values are in μM. Data are taken from Kim *et al.*[21] or the references, which are listed with parentheses.

TABLE 2

Basal reaction flux rates and associated parameters for irreversible reaction fluxes.

Fluxes	Flux rate*	$K_m^{\dagger}$	K_m†	K_i†	$\mu^{\pm\S}$	$\nu^{\pm}$ or $\eta^{\pm\S}$
$\varphi_{GLC\rightarrow G6P}$	1.88	4.06	384,000≠	210		
$\varphi_{F6P\rightarrow GAP1}$	1.96	7.83	60		0.33 (−)	
$\varphi_{GAP1\rightarrow PYR}$	3.90	31.20	27,000‡		0.33 (−)	3214 (−)
$\varphi_{G6P\rightarrow GLY}$	0.21**	0.84	210		3.02 (+)	
$\varphi_{GLY\rightarrow G6P}$	0.31**	1.24	35,100,000‡		0.33 (−)	
$\varphi_{G6P\rightarrow R5P}$	0.07**	0.28	210			3214 (−)
$\varphi_{R5P\rightarrow F6P–GAP1}$	0.07**	0.14	4			0.13 (−)§§
$\varphi_{PYR\rightarrow GAP2}$	0.38	3.01	200		3.02 (+)	0.0003 (+)
$\varphi_{GLR\rightarrow G3P2}$	0.01	0.04	220		3.02 (+)	
$\varphi_{ALA\rightarrow PYR}$	3.08	6.16	1300			
$\varphi_{PYR\rightarrow ALA}$	1.00	2.00	200			
$\varphi_{Proteolysis}$	2.65	2.65				
$\varphi_{PYR\rightarrow ACoA}$	3.92	23.52	100,000‡	25		3214 (−)
$\varphi_{FA\rightarrow FAC}$	1.71	6.86	15,000‡		3.02 (+)	
$\varphi_{FAC\rightarrow ACoA}$	0.44	2.61	14,000‡	25		3214 (−)
$\varphi_{ACoA\rightarrow FA}$	0.08**	0.64	25‡			7.63 (+)§§
$\varphi_{TG\rightarrow DG;ATGL}$	3.35	3.35				
$\varphi_{TG\rightarrow DG;HSL}$	0.65	0.65				
$\varphi_{DG\rightarrow MG;HSL}$	3.29	6.58	2000			
$\varphi_{MG\rightarrow GLR;HSL}$	0.33	0.66	200			
$\varphi_{MG\rightarrow GLR;MGL}$	2.67	29.37	2000			
$\varphi_{G3P1–FAC\rightarrow DG}$	0.04	0.08	10,500‡			
$\varphi_{G3P2–FAC\rightarrow DG}$	0.39	0.77	10,500‡			
$\varphi_{DG–FAC\rightarrow TG}$	0.43	0.85	140,000‡			
$\varphi_{DG–DG\rightarrow TG}$	0.60	1.20	2000			

Fluxes	**Flux rate***	$K_m^{\dagger}$	K_m†	K_i†	$\mu^{\pm\S}$	$\nu^{\pm}$ or $\eta^{\pm\S}$
$\varphi_{MG–MG→DG}$	0.32	0.64	200			
$\varphi_{MG–DG→TG}$	0.27	0.54	400,000‡			
$\varphi_{ACoA→CO_2}$	7.32	58.57	67,500‡		0.33 (−)	3214 (−)
$\varphi_{O_2→H_2O}$	20.43	81.73	27‡		0.33 (−)	0.0003 (+)
$\varphi_{ATP→ADP}$	129.0	258.0	3840			
$\varphi_{TG→GLR;LPL}$	0.61	1.22	990,000			

*Values are in μmol min^{-1} kg wet tissue^{-1}. $V_{max,k}$, maximum rate coefficient. Data are from the reference [21] except for those marked with **, which are from the references [37] and [47].

†Values are in μmol kg wet tissue^{-1} except for the marked (‡), which are in (μmol kg wet tissue^{-1})^2. $K_{m,k}$, phenomenological M–M constant for the reactants; $K_{i,k}$, phenomenological M–M constant for the product inhibition.

§Values are dimensionless. $\mu^{\pm}$, $\nu^{\pm}$ and $\eta^{\pm}$, parameters for the metabolic controllers. Those marked with §§, represent $\eta^{\pm}$.

(+) represents μ^{+}, ν^{+} or η^{+} while (−) represents μ^{-}, ν^{-} or η^{-}.

Cell Mol Bioeng. Author manuscript; available in PMC 2013 May 02.

TABLE 3

Basal reaction flux rates and associated parameters for reversible reaction fluxes *.

Fluxes	Flux rate	$V_{f;X\leftrightarrow V}$ †	$V_{b;X\leftrightarrow V}$ †	$K^{\ddagger}_{f,\,X\leftrightarrow V}$	$K^{\ddagger}_{b,\,X\leftrightarrow V}$	$K^{\S}_{eq,\,X\leftrightarrow V}$
$\varphi_{G6P\leftrightarrow F6P}$	1.91	42.7	37.0	210	60	0.33 **
$\varphi_{PYR\leftrightarrow LAC}$	1.55	19.7	15.1	80	648,000	1.06×10^{4}
$\varphi_{GAP1\leftrightarrow G3P1}$	0.04	0.12	7.3×10^{-6}	4	67,500	2.77×10^{8}
$\varphi_{GAP2\leftrightarrow G3P2}$	0.38	1.13	6.9×10^{-5}	4	67,500	2.77×10^{8}

* Data are from Kim *et al.*[21] except for those marked with ** which is from the reference [45].

† $V_{f,k}$ and $V_{b,k}$, forward and reverse rate coefficients (μmol min^{-1} kg wet tissue^{-1}).

‡ $K_{f,k}$ and $K_{b,k}$, phenomenological M–M constants for reactants and products (μmol kg wet tissue^{-1})2.

§ K_{eq}, equilibrium.

TABLE 4

Model input functions*.

Time (min)	Input functions
$t \leq 15$	$Q = Q_0$, $C_I = C_{I,0}$, $C_{a,GLC} = C_{a,GLC,0}$, $C_{a,LAC} = C_{a,LAC,0}$
	$C_{a,GLR} = C_{a,GLR,0}$, $C_{a,FA} = C_{a,FA,0}$, $C_{a,TG} = C_{a,TG,0}$
$t > 15$	$Q = Q_0 \cdot (1 + 7.76 \cdot (1 - e^{-(t-15)/20.54}) - 7.68 \cdot (1 - e^{-(t-15)/36.48}))$
	$C_I = C_{I,0} + 65.1 \cdot (1 - e^{-(t-15)/10})$
	$C_{a,GLC} = C_{a,GLC,0} \cdot (1 - 0.177 \cdot (t-15)^{5.26}/(22.82^{5.26} + (t-15)^{5.26}) + 0.421 \cdot (1 - e^{-(t-15)/350.3}))$
	$C_{a,LAC} = C_{a,LAC,0} \cdot (1 + 0.389 \cdot (t-15)^{7.05}/(18.88^{7.05} + (t-15)^{7.05}))$
	$C_{a,GLR} = C_{a,GLR,0} \cdot (0.41 + 0.59e^{-(t-15)/10.38})$
	$C_{a,FA} = C_{a,FA,0} \cdot (0.11 + 0.89e^{-(t-15)/17.22})$
	$C_{a,TG} = C_{a,TG,0} \cdot (1 - 0.0015 \cdot (t-15))$

* Parameters for the input functions were optimally estimated based on the data from the human *in vivo* study.[8,9,19] Q: Blood flow to the adipose tissue; C_I: Insulin concentration in the interstitial fluid; $C_{a,GLC}$, $C_{a,LAC}$, $C_{a,GLR}$, $C_{a,FA}$, $C_{a,TG}$: Arterial concentrations of glucose, lactate, glycerol, FA and TG; $C_{a,i,0}$: Initial arterial concentration of chemical species i as shown in Table 1. Time courses of these input functions are shown in Fig. 2.

TABLE 5

Estimated and miscellaneous model parameters*.

	Values	Units
Parameters for stimulative insulin actions		
$\lambda_{T_{max;GLC}}$	0.02	
$\lambda_{Glycolysis}$	5.01	
$\lambda_{Glycogen\ Synthesis}$	14.67	
λ_{PDH}	3.00	
Parameters for inhibitory insulin actions		
$\alpha_{TG \rightarrow DG,ATGL}$	70.6, 635‡	pM^2
$\alpha_{TG \rightarrow DG,HSL}$	70.6	pM^2
$\alpha_{DG \rightarrow MG,HSL}$	70.6	pM^2
$\alpha_{GLY \rightarrow G6P}$	70.6	pM^2
$\alpha_{PRT \rightarrow ALA}$	70.6	pM^2
Miscellaneous parameters		
Q_0	0.031†	ml min^{-1} kg^{-1}
$C_{I,0}$	8.4†	pM
$V_{c,i}$		
TG, DG, MG	0.8	
GAP1, GAP2, G3P1, G3P2	0.016	
Others	0.032	

*λ_k and α_k, parameter for insulin action; Q_0, adipose tissue blood flow at basal state; $C_{I,0}$, insulin concentration in the interstitial fluid at basal state. Data marked with † are from the references [18,41].

‡Two different values of $\alpha_{TG \rightarrow DG,ATGL}$ were used to simulate the different degree of suppression of ATGL reaction by insulin.

APPENDIX 1

KINETIC EQUATIONS FOR THE METABOLIC REACTIONS

1. Glycolysis I

$$\mathrm{GLC} + \mathrm{ATP} \rightarrow \mathrm{G6P} + \mathrm{ADP}$$

$$\varphi_{\mathrm{GLC}\rightarrow\mathrm{G6P}} = V_{\mathrm{GLC}\rightarrow\mathrm{G6P}} \left[\frac{K_{\mathrm{i,GLC}\rightarrow\mathrm{G6P}}}{K_{\mathrm{i,GLC}\rightarrow\mathrm{G6P}} + C_{\mathrm{G6P}}} \right] \left[\frac{\frac{C_{\mathrm{GLC}} C_{\mathrm{ATP}}}{K_{\mathrm{m,GLC}\rightarrow\mathrm{G6P}}}}{1 + \frac{C_{\mathrm{G6P}}}{K_{\mathrm{i,GLC}\rightarrow\mathrm{G6P}}} + \frac{C_{\mathrm{GLC}} C_{\mathrm{ATP}}}{K_{\mathrm{m,GLC}\rightarrow\mathrm{G6P}}}} \right]$$

2. Glycolysis II

$$\mathrm{G6P} \leftrightarrow \mathrm{F6P}$$

$$\varphi_{\mathrm{G6P}\leftrightarrow\mathrm{F6P}} = \left[\frac{V_{\mathrm{f,G6P}\leftrightarrow\mathrm{F6P}} \frac{C_{\mathrm{G6P}}}{K_{\mathrm{G6P}}} - V_{\mathrm{b,G6P}\leftrightarrow\mathrm{F6P}} \frac{C_{\mathrm{F6P}}}{K_{\mathrm{F6P}}}}{1 + \frac{C_{\mathrm{G6P}}}{K_{\mathrm{G6P}}} + \frac{C_{\mathrm{F6P}}}{K_{\mathrm{F6P}}}} \right]$$

3. Glycolysis III

$$\mathrm{F6P} + \mathrm{ATP} \rightarrow 2\mathrm{GAP1} + \mathrm{ADP}$$

$$\varphi_{\mathrm{F6P}\rightarrow\mathrm{GAP1}} = V_{\mathrm{F6P}\rightarrow\mathrm{GAP1}} \left[\frac{\left[\frac{C_{\mathrm{ADP}}}{C_{\mathrm{ATP}}} \right]^2}{\left[\mu^{-}_{\mathrm{F6P}\rightarrow\mathrm{GAP1}} \right]^2 + \left[\frac{C_{\mathrm{ADP}}}{C_{\mathrm{ATP}}} \right]^2} \right] \left[\frac{\frac{C_{\mathrm{F6P}}}{K_{\mathrm{m,F6P}\rightarrow\mathrm{GAP1}}}}{1 + \frac{C_{\mathrm{F6P}}}{K_{\mathrm{m,F6P}\rightarrow\mathrm{GAP1}}}} \right]$$

4. Glycolysis IV

$$\mathrm{GAP1} + \mathrm{Pi} + \mathrm{NAD}^{+} + 2\mathrm{ADP} \rightarrow \mathrm{PYR} + \mathrm{NADH} + 2\mathrm{ATP}$$

$$\varphi_{\mathrm{GAP1}\rightarrow\mathrm{PYR}} = V_{\mathrm{GAP1}\rightarrow\mathrm{PYR}} \left[\frac{\left[\frac{C_{\mathrm{NAD}}}{C_{\mathrm{NADH}}} \right]}{\left[\nu^{-}_{\mathrm{GAP1}\rightarrow\mathrm{PYR}} \right] + \left[\frac{C_{\mathrm{NAD}}}{C_{\mathrm{NADH}}} \right]} \right] \left[\frac{\left[\frac{C_{\mathrm{ADP}}}{C_{\mathrm{ATP}}} \right]^2}{\left[\mu^{-}_{\mathrm{GAP1}\rightarrow\mathrm{PYR}} \right]^2 + \left[\frac{C_{\mathrm{ADP}}}{C_{\mathrm{ATP}}} \right]^2} \right] \left[\frac{\frac{C_{\mathrm{GAP1}} C_{\mathrm{Pi}}}{K_{\mathrm{m,GAP1}\rightarrow\mathrm{PYR}}}}{1 + \frac{C_{\mathrm{GAP1}} C_{\mathrm{Pi}}}{K_{\mathrm{m,GAP1}\rightarrow\mathrm{PYR}}}} \right]$$

5. Pyruvate reduction

$$\mathrm{PYR} + \mathrm{NADH} \leftrightarrow \mathrm{LAC} + \mathrm{NAD}^{+}$$

$$\varphi_{\mathrm{PYR}\leftrightarrow\mathrm{LAC}} = \left[\frac{V_{\mathrm{f,PYR}\leftrightarrow\mathrm{LAC}} \frac{C_{\mathrm{PYR}} C_{\mathrm{NADH}}}{K_{\mathrm{f,PYR}\leftrightarrow\mathrm{LAC}}} - V_{\mathrm{b,PYR}\leftrightarrow\mathrm{LAC}} \frac{C_{\mathrm{LAC}} C_{\mathrm{NAD}}}{K_{\mathrm{b,PYR}\leftrightarrow\mathrm{LAC}}}}{1 + \frac{C_{\mathrm{PYR}} C_{\mathrm{NADH}}}{K_{\mathrm{f,PYR}\leftrightarrow\mathrm{LAC}}} + \frac{C_{\mathrm{LAC}} C_{\mathrm{NAD}}}{K_{\mathrm{b,PYR}\leftrightarrow\mathrm{LAC}}}} \right]$$

6. Glycogen synthesis

$$\mathrm{G6P} + \mathrm{ATP} \rightarrow \mathrm{GLY} + \mathrm{ADP} + 2\mathrm{P_i}$$

$$\varphi_{\mathrm{G6P}\rightarrow\mathrm{GLY}} = V_{\mathrm{G6P}\rightarrow\mathrm{GLY}} \left[\frac{\left[\frac{C_{\mathrm{ATP}}}{C_{\mathrm{ADP}}} \right]}{\left[\mu^{+}_{\mathrm{G6P}\rightarrow\mathrm{GLY}} \right] + \left[\frac{C_{\mathrm{ATP}}}{C_{\mathrm{ADP}}} \right]} \right] \left[\frac{\frac{C_{\mathrm{G6P}}}{K_{\mathrm{m,G6P}\rightarrow\mathrm{GLY}}}}{1 + \frac{C_{\mathrm{G6P}}}{K_{\mathrm{m,G6P}\rightarrow\mathrm{GLY}}}} \right]$$

7. Glycogen phosphorylation

$$\mathrm{GLY} + \mathrm{P_i} \rightarrow \mathrm{G6P}$$

$$\varphi_{\mathrm{GLY}\rightarrow\mathrm{G6P}} = V_{\mathrm{GLY}\rightarrow\mathrm{G6P}} \left[\frac{\left[\frac{C_{\mathrm{ADP}}}{C_{\mathrm{ATP}}} \right]^2}{\left[\mu^{-}_{\mathrm{GLY}\rightarrow\mathrm{G6P}} \right]^2 + \left[\frac{C_{\mathrm{ADP}}}{C_{\mathrm{ATP}}} \right]^2} \right] \left[\frac{\frac{C_{\mathrm{GLY}} C_{\mathrm{Pi}}}{K_{\mathrm{m,GLY}\rightarrow\mathrm{G6P}}}}{1 + \frac{C_{\mathrm{GLY}} C_{\mathrm{Pi}}}{K_{\mathrm{m,GLY}\rightarrow\mathrm{G6P}}}} \right]$$

8. Pentose phosphate shunt I

$$\mathrm{G6P} + 2\mathrm{NADP+} \rightarrow \mathrm{R5P} + 2\mathrm{NADPH} + \mathrm{CO_2}$$

$$\varphi_{\mathrm{G6P}\rightarrow\mathrm{R5P}} = V_{\mathrm{G6P}\rightarrow\mathrm{R5P}} \left[\frac{\frac{C_{\mathrm{NADP+}}}{C_{\mathrm{NADPH}}}}{\left[\eta^{-}_{\mathrm{G6P}\rightarrow\mathrm{R5P}} \right] + \left[\frac{C_{\mathrm{NADP+}}}{C_{\mathrm{NADPH}}} \right]} \right] \left[\frac{\frac{C_{\mathrm{G6P}}}{K_{\mathrm{m,G6P}\rightarrow\mathrm{R5P}}}}{1 + \frac{C_{\mathrm{G6P}}}{K_{\mathrm{m,G6P}\rightarrow\mathrm{R5P}}}} \right]$$

9. Pentose phosphate shunt II

$$3\mathrm{R5P} \rightarrow 2\mathrm{F6P} + \mathrm{GAP1}$$

$$\varphi_{R5P\to F6P-GAP1}=V_{R5P\to F6P-GAP1}\left[\frac{\frac{C_{R5P}}{K_{m,R5P\to F6P-GAP1}}}{1+\frac{C_{R5P}}{K_{m,R5P\to F6P-GAP1}}}\right]$$

10. GAP reduction I

$$\text{GAP1} + \text{NADH} \leftrightarrow \text{G3P1} + \text{NAD}^+$$

$$\varphi_{GAP1\leftrightarrow G3P1}=\left[\frac{V_{f,GAP1\leftrightarrow G3P1}\frac{C_{GAP1}C_{NADH}}{K_{f,GAP1\leftrightarrow G3P1}}-V_{b,GAP1\leftrightarrow G3P1}\frac{C_{G3P1}C_{NAD}}{K_{b,GAP\leftrightarrow G3P1}}}{1+\frac{C_{GAP1}C_{NADH}}{K_{f,GAP1\leftrightarrow G3P1}}+\frac{C_{G3P1}C_{NAD}}{K_{b,GAP1\leftrightarrow G3P1}}}\right]$$

11. Glyceroneogenesis

$$\text{PYR} + 3\text{ATP} + \text{NADH} \rightarrow \text{GAP2} + 3\text{ADP} + \text{NAD}^+ + 2\text{P}_i$$

$$\varphi_{PYR\to GAP2}=V_{PYR\to GAP2}\left[\frac{\left[\frac{C_{NADH}}{C_{NAD+}}\right]}{\nu^+_{PYR\to GAP2}+\left[\frac{C_{NADH}}{C_{NAD+}}\right]}\right]\left[\frac{\frac{C_{ATP}}{C_{ADP}}}{\left[\mu^+_{PYR\to GAP2}\right]+\left[\frac{C_{ATP}}{C_{ADP}}\right]}\right]\left[\frac{\frac{C_{PYR}}{K_{m,PYR\to GAP2}}}{1+\frac{C_{PYR}}{K_{m,PYR\to GAP2}}}\right]$$

12. GAP reduction II

$$\text{GAP2} + \text{NADH} \leftrightarrow \text{G3P2} + \text{NAD}^+$$

$$\varphi_{GAP2\leftrightarrow G3P2}=\left[\frac{V_{f,GAP2\leftrightarrow G3P2}\frac{C_{GAP2}C_{NADH}}{K_{f,GAP2\leftrightarrow G3P2}}-V_{b,GAP2\leftrightarrow G3P2}\frac{C_{G3P2}C_{NAD}}{K_{b,GAP2\leftrightarrow G3P2}}}{1+\frac{C_{GAP2}C_{NADH}}{K_{f,GAP2\leftrightarrow G3P2}}+\frac{C_{G3P2}C_{NAD}}{K_{b,GAP2\leftrightarrow G3P2}}}\right]$$

13. Glycerol phosphorylation

$$\text{GLR} + \text{ATP} \rightarrow \text{G3P2} + \text{ADP}$$

$$\varphi_{GLR\to G3P2}=V_{GLR\to G3P2}\left[\frac{\left[\frac{C_{ATP}}{C_{ADP}}\right]}{\left[\mu^+_{GLR\to G3P2}\right]+\left[\frac{C_{ATP}}{C_{ADP}}\right]}\right]\left[\frac{\frac{C_{GLR}}{K_{m,GLR\to G3P2}}}{1+\frac{C_{GLR}}{K_{m,GLR\to G3P2}}}\right]$$

14. Alanine utilization

$$\text{ALA} \rightarrow \text{PYR}$$

$$\varphi_{ALA\to PYR}=V_{ALA\to PYR}\left[\frac{\frac{C_{ALA}}{K_{m,ALA\to PYR}}}{1+\frac{C_{ALA}}{K_{m,ALA\to PYR}}}\right]$$

Alanine represents the amino acid pool.

15. Alanine formation

$$\text{PYR} \rightarrow \text{ALA}$$

$$\varphi_{PYR\to ALA}=V_{PYR\to ALA}\left[\frac{\frac{C_{PYR}}{K_{m,PYR\to ALA}}}{1+\frac{C_{PYR}}{K_{m,PYR\to ALA}}}\right]$$

16. Proteolysis

$$\text{Proteins} \rightarrow \text{ALA}$$

$$\varphi_{Proteolysis}=V_{Proteolysis}$$

17. Protein synthesis

$$\text{ALA} \rightarrow \text{Proteins}$$

$$\varphi_{ProteinSynthesis}=V_{ProteinSynthesis}$$

18. Pyruvate oxidation

$$\text{PYR} + \text{CoA} + \text{NAD}^+ \rightarrow \text{ACoA} + \text{NADH} + \text{CO}_2$$

$$\varphi_{PYR\to ACoA}=V_{PYR\to ACoA}\left[\frac{\left[\frac{C_{NAD}}{C_{NADH}}\right]}{\left[\nu^-_{PYR\to ACoA}\right]+\left[\frac{C_{NAD}}{C_{NADH}}\right]}\right]\left[\frac{\frac{C_{PYR}C_{CoA}}{K_{m,PYR\to ACoA}}}{1+\frac{C_{ACoA}}{K_{i,PYR\to ACoA}}+\frac{C_{PYR}C_{CoA}}{K_{m,PYR\to ACoA}}}\right]$$

19. Fatty Acyl CoA synthesis

$$\text{FFA} + \text{CoA} + 2\text{ATP} \rightarrow \text{FAC} + 2\ \text{ADP} + 2\ \text{Pi}$$

$$\varphi_{\mathrm{FFA}\to\mathrm{FAC}} = V_{\mathrm{FFA}\to\mathrm{FAC}} \left[\frac{\left[\frac{C_{\mathrm{ATP}}}{C_{\mathrm{ADP}}}\right]}{\left[\mu^{+}_{\mathrm{FFA}\to\mathrm{FAC}}\right] + \left[\frac{C_{\mathrm{ATP}}}{C_{\mathrm{ADP}}}\right]} \right] \left[\frac{\frac{C_{\mathrm{FFA}} C_{\mathrm{CoA}}}{K_{\mathrm{m,FFA}\to\mathrm{FAC}}}}{1 + \frac{C_{\mathrm{FFA}} C_{\mathrm{CoA}}}{K_{\mathrm{m,FFA}\to\mathrm{FAC}}}} \right]$$

20. Fatty acid oxidation

$$\mathrm{FAC} + 7\mathrm{CoA} + 14\mathrm{NAD}^{+} \rightarrow 8\mathrm{ACoA} + 14\mathrm{NADH}$$

$$\varphi_{\mathrm{FAC}\to\mathrm{ACoA}} = V_{\mathrm{FAC}\to\mathrm{ACoA}} \left[\frac{\left[\frac{C_{\mathrm{NAD+}}}{C_{\mathrm{NADH}}}\right]}{\left[\gamma^{-}_{\mathrm{FAC}\to\mathrm{ACoA}}\right] + \left[\frac{C_{\mathrm{NAD+}}}{C_{\mathrm{NADH}}}\right]} \right] \left[\frac{\frac{C_{\mathrm{FAC}} C_{\mathrm{CoA}}}{K_{\mathrm{m,FAC}\to\mathrm{ACoA}}}}{1 + \frac{C_{\mathrm{ACoA}}}{K_{\mathrm{i,FAC}\to\mathrm{ACoA}}} + \frac{C_{\mathrm{FAC}} C_{\mathrm{CoA}}}{K_{\mathrm{m,FAC}\to\mathrm{ACoA}}}} \right]$$

21. TG breakdown by ATGL

$$\mathrm{TG} \rightarrow \mathrm{DG} + \mathrm{FFA}$$

$$\varphi_{\mathrm{TG}\to\mathrm{DG}} = V_{\mathrm{TG}\to\mathrm{DG,ATGL}}$$

22. TG breakdown by HSL

$$\mathrm{TG} \rightarrow \mathrm{DG} + \mathrm{FFA}$$

$$\varphi_{\mathrm{TG}\to\mathrm{DG}} = V_{\mathrm{TG}\to\mathrm{DG,HSL}}$$

23. DG breakdown by HSL

$$\mathrm{DG} \rightarrow \mathrm{MG} + \mathrm{FFA}$$

$$\varphi_{\mathrm{DG}\to\mathrm{MG}} = V_{\mathrm{DG}\to\mathrm{MG,HSL}} \left[\frac{\frac{C_{\mathrm{DG}}}{K_{\mathrm{m,DG}\to\mathrm{MG}}}}{1 + \frac{C_{\mathrm{DG}}}{K_{\mathrm{m,DG}\to\mathrm{MG}}}} \right]$$

24. MG breakdown by HSL

$$\mathrm{MG} \rightarrow \mathrm{GLR} + \mathrm{FFA}$$

$$\varphi_{\mathrm{MG}\to\mathrm{GLR}} = V_{\mathrm{MG}\to\mathrm{GLR,HSL}} \left[\frac{\frac{C_{\mathrm{MG}}}{K_{\mathrm{m,MG}\to\mathrm{GLR}}}}{1 + \frac{C_{\mathrm{MG}}}{K_{\mathrm{m,MG}\to\mathrm{GLR}}}} \right]$$

25. MG breakdown by MGL

$$\mathrm{MG} \rightarrow \mathrm{GLR} + \mathrm{FFA}$$

$$\varphi_{\mathrm{MG}\to\mathrm{GLR}} = V_{\mathrm{MG}\to\mathrm{GLR,MGL}} \left[\frac{\frac{C_{\mathrm{MG}}}{K_{\mathrm{m,MG}\to\mathrm{GLR}}}}{1 + \frac{C_{\mathrm{MG}}}{K_{\mathrm{m,MG}\to\mathrm{GLR}}}} \right]$$

26. Lipogenesis

$$8\mathrm{ACoA} + 14\mathrm{NADPH} + 7\mathrm{ATP} \rightarrow \mathrm{FFA} + 8\mathrm{CoA} + 14\mathrm{NADP} + 7\mathrm{ADP} + 7\mathrm{P_i}$$

$$\varphi_{\mathrm{ACoA}\to\mathrm{FFA}} = V_{\mathrm{ACoA}\to\mathrm{FFA}} \left[\frac{\left[\frac{C_{\mathrm{ATP}}}{C_{\mathrm{ADP}}}\right]}{\left[\mu^{+}_{\mathrm{ACoA}\to\mathrm{FFA}}\right] + \left[\frac{C_{\mathrm{ATP}}}{C_{\mathrm{ADP}}}\right]} \right] \left[\frac{\left[\frac{C_{\mathrm{NADPH}}}{C_{\mathrm{NADP+}}}\right]}{\left[\eta^{+}_{\mathrm{ACoA}\to\mathrm{FFA}}\right] + \left[\frac{C_{\mathrm{NADPH}}}{C_{\mathrm{NADP+}}}\right]} \right] \left[\frac{\frac{C_{\mathrm{ACoA}}}{K_{\mathrm{m,ACoA}\to\mathrm{FFA}}}}{1 + \frac{C_{\mathrm{ACoA}}}{K_{\mathrm{m,ACoA}\to\mathrm{FFA}}}} \right]$$

27. DG synthesis I

$$\mathrm{G3P1} + 2\mathrm{FAC} \rightarrow \mathrm{DG} + 2\mathrm{CoA} + \mathrm{Pi}$$

$$\varphi_{\mathrm{G3P1-FAC}\to\mathrm{DG}} = V_{\mathrm{G3P1-FAC}\to\mathrm{DG}} \left[\frac{\frac{C_{\mathrm{G3P1}} C_{\mathrm{FAC}}}{K_{\mathrm{m,G3P1-FAC}\to\mathrm{DG}}}}{1 + \frac{C_{\mathrm{G3P1}} C_{\mathrm{FAC}}}{K_{\mathrm{m,G3P1-FAC}\to\mathrm{DG}}}} \right]$$

28. DG synthesis II

$$\mathrm{G3P2} + 2\mathrm{FAC} \rightarrow \mathrm{DG} + 2\mathrm{CoA} + \mathrm{Pi}$$

$$\varphi_{\mathrm{G3P2-FAC}\to\mathrm{DG}} = V_{\mathrm{G3P2-FAC}\to\mathrm{DG}} \left[\frac{\frac{C_{\mathrm{G3P2}} C_{\mathrm{FAC}}}{K_{\mathrm{m,G3P2-FAC}\to\mathrm{DG}}}}{1 + \frac{C_{\mathrm{G3P2}} C_{\mathrm{FAC}}}{K_{\mathrm{m,G3P2-FAC}\to\mathrm{DG}}}} \right]$$

29. TG synthesis

$$\mathrm{DG} + \mathrm{FAC} \rightarrow \mathrm{TG} + \mathrm{CoA}$$

$$\varphi_{DG-FAC\rightarrow TG} = V_{DG-FAC\rightarrow TG}\left[\frac{\frac{C_{DG}C_{FAC}}{K_{m,DG-FAC\rightarrow TG}}}{1+\frac{C_{DG}C_{FAC}}{K_{m,DG-FAC\rightarrow TG}}}\right]$$

30. Transacylation I

$$DG + DG \rightarrow TG + MG$$

$$\varphi_{DG-DG\rightarrow TG-MG} = V_{DG-DG\rightarrow TG-MG}\left[\frac{\frac{C_{DG}}{K_{m,DG-DG\rightarrow TG-MG}}}{1+\frac{C_{DG}}{K_{m,DG-DG\rightarrow TG-MG}}}\right]$$

31. Transacylation II

$$MG + MG \rightarrow DG + GLR$$

$$\varphi_{MG-MG\rightarrow DG-GLR} = V_{MG-MG\rightarrow DG-GLR}\left[\frac{\frac{C_{MG}}{K_{m,MG-MG\rightarrow DG-GLR}}}{1+\frac{C_{MG}}{K_{m,MG-MG\rightarrow DG-GLR}}}\right]$$

32. Transacylation III

$$MG + DG \rightarrow TG + GLR$$

$$\varphi_{MG-DG\rightarrow TG-GLR} = V_{MG-DG\rightarrow TG-GLR}\left[\frac{\frac{C_{MG}C_{DG}}{K_{m,MG-DG-TG-GLR}}}{1+\frac{C_{MG}C_{DG}}{K_{m,MG-DG\rightarrow TG-GLR}}}\right]$$

33. TCA cycle

$$ACoA + ADP + Pi + 4NAD^{+} \rightarrow 2CO_2 + CoA + ATP + 4NADH$$

$$\varphi_{ACoA\leftrightarrow CO_2} = V_{ACoA\leftrightarrow CO_2}\left[\frac{\left[\frac{C_{NAD+}}{C_{NADH}}\right]}{\left[\nu^{-}_{ACoA\rightarrow CO_2}\right]+\left[\frac{C_{NAD+}}{C_{NADH}}\right]}\right]\left[\frac{\left[\frac{C_{ADP}}{C_{ATP}}\right]}{\left[\mu^{-}_{ACoA\rightarrow CO_2}\right]+\left[\frac{C_{ADP}}{C_{ATP}}\right]}\right]\left[\frac{\frac{C_{ACoA}C_{Pi}}{K_{m,ACoA\rightarrow CO_2}}}{1+\frac{C_{ACoA}C_{Pi}}{K_{m,ACoA\rightarrow CO_2}}}\right]$$

34. Oxidative phosphorylation

$$O_2 + 6ADP + 6Pi + 2NADH \rightarrow 2H_2O + 6ATP + 2NAD^{+}$$

$$\varphi_{O_2\rightarrow H_2O} = V_{O_2\rightarrow H_2O}\left[\frac{\left[\frac{C_{NADH}}{C_{NAD+}}\right]}{\left[\nu^{+}_{O_2\rightarrow H_2O}\right]+\left[\frac{C_{NAD+}}{C_{NADH}}\right]}\right]\left[\frac{\left[\frac{C_{ADP}}{C_{ATP}}\right]}{\left[\mu^{-}_{O_2\rightarrow H_2O}\right]+\left[\frac{C_{ADP}}{C_{ATP}}\right]}\right]\left[\frac{\frac{C_{O_2}C_{Pi}}{K_{m,O_2\rightarrow H_2O}}}{1+\frac{C_{O_2}C_{Pi}}{K_{m,O_2\rightarrow H_2O}}}\right]$$

35. ATP hydrolysis

$$ATP \rightarrow ADP + Pi$$

$$\varphi_{ATP\rightarrow ADP} = V_{ATP\rightarrow ADP}\left[\frac{\frac{C_{ATP}}{K_{ATP\rightarrow ADP}}}{1+\frac{C_{Pi}C_{ADP}}{K_{i,ATP\rightarrow ADP}}+\frac{C_{ATP}}{K_{m,ATP\rightarrow ADP}}}\right]$$

36. TG breakdown by LPL

$$TG \rightarrow GLR + 3FFA$$

$$\varphi_{TG\rightarrow FFA,LPL} = V_{TG\rightarrow FFA,LPL}\left[\frac{\frac{C_{TG}}{K_{m,TG\rightarrow FFA,LPL}}}{1+\frac{C_{TG}}{K_{m,TG\rightarrow FFA,LPL}}}\right]$$

This is the only reaction in the blood compartment which is governed by LPL. Rate coefficient is activated by adipose blood flow.